Impingement Splattering and Surface Disturbance Evolution on Turbulent Liquid Jets in Gases

by

Sourav Kumar Bhunia

B.Tech.(Hons.), Indian Institute of Technology, Kharagpur (1986)
M.S., Case Western Reserve University (1988)

Submitted to the Department of Mechanical Engineering
in partial fulfillment of the requirements for the degree of

Doctor of Philosophy in Mechanical Engineering

at the

MASSACHUSETTS INSTITUTE OF TECHNOLOGY

June 1993

Author . . . .
Department of Mechanical Engineering
June 28, 1993

Certified by . . . . . / . . . . ᴠ. . ᴢ. . . . .
John H. Lienhard V
Associate Professor
Thesis Supervisor

Accepted by . . . .
Professor Ain A. Sonin
Chairman, Departmental Committee on Graduate Studies

Impingement Splattering and Surface Disturbance Evolution on Turbulent Liquid Jets in Gases

by

Sourav Kumar Bhunia

Abstract

Splattering of droplets during liquid jet impingement on solid targets alters the efficiencies of jet impingement heat transfer processes and chemical containment safety devices, and leads to problems of aerosol formation in jet impingement cleaning processes. A study of the turbulent liquid jet impingement splattering, the evolution of the disturbances on the free surface of a turbulent liquid jet in gas and the relation between splattering and the jet surface disturbances is presented here.

Experimental results on the amount of splattering for jets of water, isopropanol-water solutions, and soap-water mixtures are reported here. Jets were produced by straight tube nozzles of diameter $0.8 - 5.8$ mm, with fully-developed turbulent pipe-flow upstream of the nozzle exit. These experiments cover Weber numbers between $130 - 31,000$, Reynolds numbers between $2700 - 98,000$, and nozzle-to-target separations of $0.2 \leq x/d \leq 125$. Splattering of up to 75% of the incoming jet liquid is observed. The results show that only the Weber number and x/d affect the fraction of jet liquid splattered. The presence of surfactants does not alter the splattering. Also a new correlation for the onset condition for splattering is presented.

A laser-based optical technique is used to measure the amplitudes of surface disturbances on turbulent liquid jets in air. Measurements were made on jets of water, isopropanol-water solutions, soap-water mixtures and water with drag reducing additive, guar, between 0.2 and 50 nozzle diameters from the nozzle. Measurements show a non-exponential growth of the rms amplitude of the surface disturbances on the jet as it moves downstream. Power spectra of the surface disturbances show the broadband turbulent disturbances to be dominant over any single wavenumber Rayleigh-type instability. The measured rms amplitude of roughness on the jet surface correlates well with the fraction of impinging liquid splattered.

A mathematical model of free surface turbulence is presented. The spectrum of disturbances is calculated based on the pressure spectrum of isotropic, homogeneous turbulence. Both the theoretical model and the experiments show that the high-wavenumber portion of the spectrum decays as $k^{-19/3}$ owing to the damping effect of capillary pressure on the turbulent pressure spectrum that drives surface roughening.

A mathematical model for the growth of turbulent disturbances on a free-surface liquid jet is also proposed.

To,

my parents Hirendranath and Mira

and

my wife Anuradha

Acknowledgements

I would like to thank my thesis supervisor Professor John H. Lienhard V for all his help and guidance. His knowledge and a passion for thoroughness have been the most important contributing factors towards improving the quality of this research. I must mention my appreciation for the opportunities he provided his students by taking them to the professional meetings and conferences and introducing them to their professional community. I would like to thank Professor Ain A. Sonin for his help as a member of my thesis committee and the brief opportunity I had to work with him. I would also like to thank Professor Roger D. Kamm for the very useful suggestions he made as a member of the thesis committee.

My stay at MIT has been enriched by so many wonderful people I have met here. To my fellow graduate students in the Fluid Mechanics and the Heat Transfer laboratories especially, Steve Brown, Manuel Cruz, Jayanta Kapat, Martitia Barsotti, Hamdi Kozlu, Dave Otis, Jamie Geshwind, Frank Espinosa, Serhat Yesilyurt, my best wishes. Thanks to Donna Wilker for all the stimulating discussions outside the scope of mechanical engineering. Many thanks to Virginia Brambilla, Lucille Blake and Claire Sasahara for their help.

Thanks to Norman MacAskill for his cheerful help many times during this project.

Now at the close of my formal education, my sincere gratitude to my parents, who set me on the course and supported and encouraged through it. They have borne silently the grief of separation for years at a stretch.

After being away and for the first time not seeing her parents for over three years, my wife had an opportunity to visit them. Knowing fully well that because of visa regulations the next such opportunity may be years away, she declined because she wanted to be with me during the presentation and submission of my thesis. I can thank her for her occasional help with running the experiments and entering data into the computer but I cannot express my gratitude for her encouragement and support.

5

Contents

List of Figures

8

9

10

List of Tables

Nomenclature

a	jet radius (m)
$\mathcal{D}$	diffusion coefficient (m²/s)
d	nozzle diameter (m)
f	Darcy friction factor
$G(\eta_p)$	spectrum of the amplitude of free surface disturbances (Equation 3.8)
h_D	coefficient of mass transfer (kg/m².s)
J	surface concentration of adsorbed mass (kg/m²)
j	mass flux (kg/m².s)
k	wavenumber (1/m)
k_1, k_2, k_3	Cartesian components of the wavenumber vector corresponding to x, y, z directions, respectively, $k^2 = k_1^2 + k_2^2 + k_3^2$ (1/m)
k_p	resultant wavenumber in the x-y plane, $\sqrt{k_1^2 + k_2^2}$ (1/m)
l	integral scale of turbulence (m)
l_b	jet breakup length (m)
l_c	length of the jet at which splattering reaches its asymptotic limit (m)
l_o	length of the jet corresponding to onset of splattering (5% threshold) (m)
m_∞	bulk mass fraction of the solute

p	fluctuating component of pressure (N/m^2)
$\tilde{p}$	$p - \sigma/a$ (N/m^2)
Q	jet flow rate (m^3/s)
Q_s	flow rate of splattered liquid (m^3/s)
u	jet free surface velocity (m/s)
u_f	average jet velocity at the nozzle exit (m/s)
u'	rms fluctuating component of velocity (m/s)
u_*	friction velocity based on wall shear stress, $u_f\sqrt{f/8}$ (m/s)
x	nozzle-to-target separation or distance along the jet axis from the nozzle exit (m)
δ	instantaneous height of the jet surface disturbances (m)
$\overline{\delta^2}$	ensemble average of δ^2 (m^2)
λ	jet surface disturbance wavelength (m)
μ	liquid dynamic viscosity (kg/m.s)
ν	liquid kinematic viscosity, μ/ρ (m^2/s)
ξ	splattered fraction of incoming jet's liquid, Q_s/Q
ρ	liquid or solution density (kg/m^3)
η	dimensionless wavenumber, kl (ka in Appendix B)
η_p	dimensionless wavenumber of the free surface disturbances, $l\sqrt{k_1^2 + k_2^2}$
σ	surface tension between jet liquid and the surrounding gas (N/m)
ω	splattering parameter defined by Equation 2.2
Re$_d$	jet Reynolds number, $\rho u_f d/\mu$
Re$_t$	turbulent Reynolds number, $u'l/\nu$
Sc	Schmidt number, $\nu/\mathcal{D}$
Sh$_t$	turbulent Sherwood number, $h_D l/\rho\mathcal{D}$
We$_d$	jet Weber number, $\rho u_f^2 d/\sigma$

Chapter 1

Introduction

When a turbulent liquid jet in air impinges on a flat target a spray of droplets break off from the liquid layer formed on the target. This splattering of droplets lowers the efficiency of jet impingement cooling processes due to the loss of liquid. It also leads to aerosol formation in jet cleaning processes and in some chemical containment safety devices where a leaking chemical stream strikes a solid object. In cleanroom situations, where impinging jets are used for post-etching debris removal, splattered liquid can produce airborne contaminants. In metal-jet forming operations, splattering is a primary cause of reduced yield. In situations involving toxic chemicals, the splattered droplets create a hazardous aerosol whose containment may necessitate significant air filtration costs. The present and earlier studies indicated a dependence of the amount of splattering on the level of jet surface disturbances. This research concentrated on studying the process of splattering, the amplitude of disturbances on the free surfaces of turbulent jets and the relation between the two.

Errico (1986) first made some of the preliminary observations and measurements of jet impingement splattering. He reported that a smooth laminar jet impinging on a solid target does not splatter. Though he noticed that naturally "rough" turbulent jets cause splattering upon impingement, he did not consider turbulence to be an important factor in splattering. Applying lateral electric fields, Errico showed that the laminar jets also can be made to cause splattering by externally imposing surface disturbances. So he concluded that the jet surface disturbance is the cause of jet

impingement splattering. He also measured the amount of splattering but all the measurements were made at fixed distance of 40 cm between the nozzle and the target.

Lienhard, Liu and Gabour (1992) reported systematic measurements of the amount of splattering for turbulent jets. They made direct measurements by capturing the amount of liquid remaining on the liquid film on the target after splattering. Measurements were also made using Phase Doppler Particle Analyzer (PDPA) where the amount of splattering was obtained by integrating the local measurements of droplet flow rate. But the PDPA measurements were found to be less accurate than the direct measurements of splattering. They proposed a model of the growth of the rms amplitude of disturbances on turbulent liquid jets in gases assuming the turbulent disturbances to grow at the highest disturbance growth rate predicted be Rayleigh's theory. The measurements of the fraction of jet liquid splattered were correlated with the rms amplitude of turbulent jet surface disturbances predicted by their model. But the scope of their measurements were rather limited. Also the assumption of the growth rate of the turbulent disturbances to be same as the highest growth rate of Rayleigh model is inadequate because the highest growth rate of Rayleigh model occurs for a disturbance wavelength longer than the jet diameter whereas most of the energetic turbulent disturbances have wavelengths shorter than the jet diameter.

Womac, Aharoni, Ramadhyani and Incropera (1990) reported a few measurements of the onset conditions for splattering of jets of water and FC-77 (a fluorocarbon chemical compound used in cooling electronic circuits). Their measurements were found consistent with the correlation proposed in this study (Section 2.3.3).

Many phenomena associated with turbulent liquid jets in gases are controlled by the free surface disturbances. The amount of splattering in jet impingement depends on the amplitude of the turbulent jet surface disturbances. The breakup of free-surface turbulent liquid jets and spray formation, adsorption onto and evaporation from turbulent liquid jets (Kim and Mills, 1989a) also depend on the surface disturbances. There are several axiomatic models of the axial and radial decay of turbulence in free-surface turbulent liquid jets (see Kim and Mills, 1989b). But the lack of quan-

titative measurements on the turbulent free-surface liquid jets, both cylindrical and planar, is well known (Wolf, Viskanta and Incropera, 1990).

The only attempt at a quantitative study of the amplitude of disturbances on the free surface of turbulent liquid jets, that the author has found in literature, was made by Chen and Davis (1964). They used an electric conductivity probe where a needle indicated the location of the free surface of the jet upon contact. The accuracy of the small number of measurements that they made was severely limited by the interference of the probe with the flow. During the current study observations with a reconstructed probe of the type they used, indicated liquid-drop formation on the probe tip. That leads to the possibility of over-estimation of the amplitudes of surface disturbances by this technique.

Stevens and Webb (1991b) reported a few measurements of the velocity on the jet free surface along the axial direction, using a Laser Doppler Velocimeter (LDV). Apparently because of the increasing amplitude of disturbances their measurements were restricted to mostly within a distance of 3 nozzle diameters from the nozzle exit. They found that the jet free surface velocity reached 90% of the average jet velocity within that distance for the jets in their study.

Chapter 2

Splattering during Turbulent Liquid Jet Impingement on Solid Targets

2.1 Introduction

Previous studies of splattering have demonstrated that it is driven by the disturbances on the surface of the impinging jet (Errico, 1986; Lienhard, Liu and Gabour, 1992). Thus, undisturbed laminar jets do not splatter, unless they are long enough to have developed significant disturbances from capillary instability. Turbulent jets, on the other hand, develop surface roughness as a result of liquid-side pressure fluctuations driven by the turbulence, and they are highly susceptible to splattering.

Errico (1986) induced splattering of laminar jets by creating surface disturbances with a fluctuating electric field. His results showed that splattering commenced at progressively lower jet velocities when the amplitude of disturbance was increased. He also showed that splattering appeared on the liquid film on the target as the disturbances from the jet spread radially. When a turbulent jet strikes a target, similar travelling waves originate near the impingement point and travel outward on the liquid film (see Figure 1b of Lienhard, Liu and Gabour 1992). When the jet disturbances are sufficiently large, these waves sharpen and break into droplets
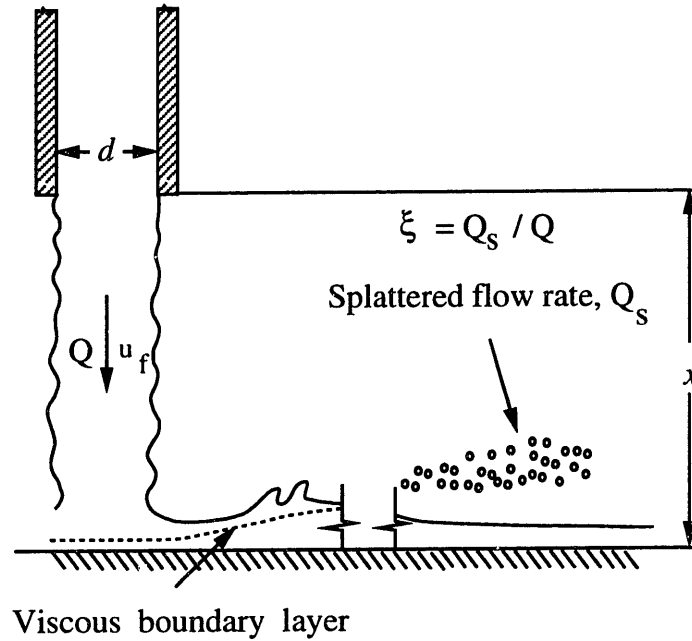
Figure 2-1: Turbulent jet impingement and splattering : instantaneous liquid surface.

(Figure 2-1). All observations indicate that the amplitude of the disturbances on the jet govern splattering. They further indicate that splattering is a non-linear instability phenomenon, since the liquid film is clearly stable to small disturbances but unstable to large ones (Varela and Lienhard, 1991).

Lienhard, Liu and Gabour (1992; called LLG hereinafter) reported measurements of the splattered liquid flow rate for turbulent jets, in the form of the ratio of splattered flow rate, Q_s to the incoming flow rate, Q:

$$\xi = \frac{Q_s}{Q} \qquad (2.1)$$

LLG also proposed a model for splattering which related the rms amplitude of jet surface disturbances to the rate of splattering. In this model, turbulent pressure fluctuations in the jet formed an initial surface disturbance on the jet, which was

18

then assumed to evolve by Rayleigh's capillary instability (Drazin and Reid, 1981) as the jet travelled to the target. The model produced a scaling parameter, ω, which characterized the rms amplitude of disturbances reaching the target:

$$\omega = \text{We}_d \exp\left(\frac{.971}{\sqrt{\text{We}_d}}\frac{x}{d}\right) \tag{2.2}$$

Here,

$$\text{We}_d = \rho u_f^2 d/\sigma \tag{2.3}$$

is the jet Weber number based on the average jet-velocity at the nozzle exit, u_f, the nozzle diameter[1], d, and the liquid surface tension, σ. The nozzle-to-target separation is x [2]. LLG obtained good correlation between ξ and ω, leading to the result:

$$\xi = -0.0935 + 3.41 \times 10^{-5}\omega + 2.25 \times 10^{-9}\omega^2 \tag{2.4}$$

for $2120 \leq \omega \leq 8000$, with no splattering for $\omega < 2120$. LLG also noted that splattering occurred within a few diameters of the point of impact and that viscosity (in the form of a jet Reynolds number) appeared to have no role in the splattering process, presumably owing to the thinness of the wall boundary layer in the stagnation region.

In spite of the LLG model's apparent success, several ambiguities accompany it. The model is based on data covering $1.2 \leq x/d \leq 28.7$ and $1000 \leq \text{We}_d \leq 5000$, and its validity beyond that range is unestablished. The onset point for splattering shows significant scatter as a function of ω and is not in complete agreement with all observations by other investigators. Furthermore, the model is predicated on exponential growth of capillary disturbances at the rate corresponding to Rayleigh analysis' most unstable wavelength ($\lambda = 4.51d$). That assumption is obviously flawed, since the turbulent pressure fluctuations driving instability cover a broad range of

---

[1]The contraction coefficient for turbulent jets leaving pipe nozzles is nearly unity. Throughout this study, we treat nozzle diameter and jet diameter interchangeably.

[2]x is being used instead of l used by LLG, since the location of the target on jet axis, x, is same as the nozzle-to-target separation.

much shorter wavelengths ($\lambda < d$), the most energetic of which should be *stable* according to Rayleigh's results.

The present study examines splattering over a much broader range of Weber number and nozzle-to-target separations ($130 < \text{We}_d < 31,000$; $0.2 < x/d < 125$). Surface tension is independently varied. In contrast to LLG, we treat We_d and x/d as independent parameters. Our objectives are to establish the range of applicability of the LLG model and to obtain a more generally applicable criterion for the onset of splattering beneath a turbulent impinging liquid jet. In addition, we attempt further explanation of the overall phenomenon of splattering in terms of the available data on the evolution of surface-disturbances on turbulent jets.

2.2 Experiments

A schematic diagram of the measurement system is given in Figure 2-2. All the measurements were made with water jets issuing into still air. Tube nozzles having diameters between 0.8 – 5.8 mm were used to produce the jets. The tubes were made 70 – 100 diameters long so as to ensure fully-developed turbulent flow at the tube outlet. The outlets were carefully deburred to prevent the introduction of mechanical surface disturbances. The tube nozzles received water from a pressurized plenum with disturbance dampeners and honeycomb flow straighteners at its upstream inlet.

Nozzle-target separation was varied from 2 to 300 mm. This corresponds to nondimensional nozzle-target separations, x/d, between 0.2 and 125 for all the nozzles other than the 0.84 mm diameter nozzle, for which x/d reached 500.

Splattering takes place over a limited range of radial positions upstream of the hydraulic jump, typically within a few diameters of the point of impact. The target radius was between 2 and 50 cm, and always slightly larger than the radial location of the hydraulic jump. The amount of liquid that remained in the liquid sheet on the target after splattering was measured by collecting it in a container beneath the target. The splattered liquid, on the other hand, remained airborne and fell well beyond the rim of the container. Flow rates of the jet and of the unsplattered liquid

20
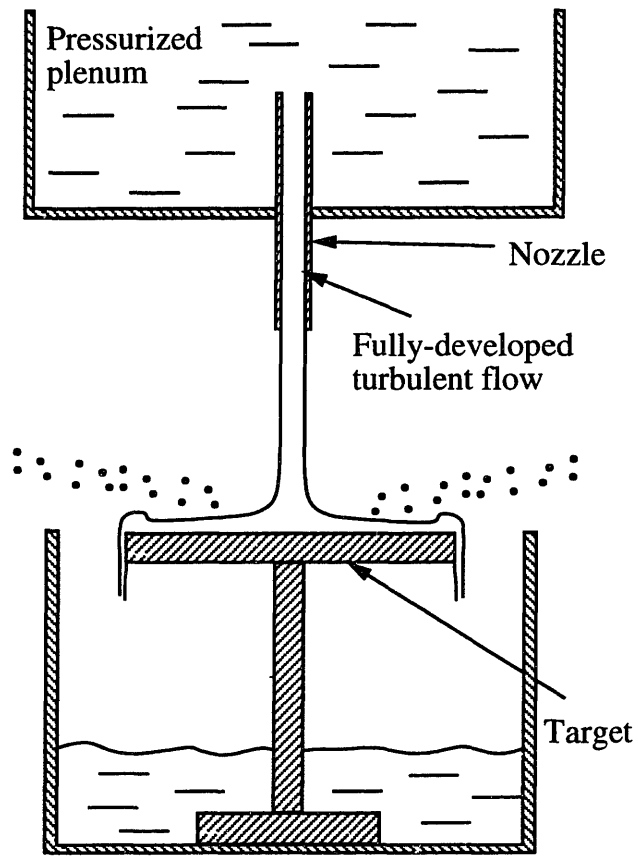
Figure 2-2: Measurement of the fraction of jet liquid splattered.

were both obtained by measuring the time required to collect a known volume of liquid. From this, the amount of splattering was calculated.

The liquids used in these experiments were water, an isopropanol-water solution, and water containing a surfactant, detergent. The liquid temperature was between 21 and 27°C. Surface tension was measured several times during the experiments using a platinum-ring surface tension meter. Tube diameters were measured and checked for roundness, and these measured values of diameter were used in all subsequent calculations.

This technique facilitated quite precise measurements of the amount of splattering. Typically the uncertainty in ξ (at 95% confidence) was below $\pm 5\%$ for $\xi > 10\%$ and below $\pm 25\%$ for $\xi < 4\%$. Uncertainties in the Reynolds numbers and the Weber numbers were below $\pm 2\%$ and $\pm 3\%$, respectively. These low uncertainties may be credited to the direct measurement of liquid flow rate. Uncertainties in x/d and ω were below $\pm 2\%$ and $\pm 3\%$, respectively. Some of the measurements were repeated using two different pumps to verify the reproducibility of the data and their independence from upstream pressure fluctuations. Figure 2-3 shows the typical scatter in the measurements of splatter fraction for several different runs at nearly same jet Weber numbers (the values are all within the $\pm 3\%$ uncertainty limits of We_d). The rms scatter in ξ from run to run is $\pm 4\%$ of the maximum value of ξ of about 0.3.

The independent physical parameters involved in this problem are x, d, ρ, u_f, σ, and μ. Dimensional analysis based on these parameters shows that the fraction of liquid splattered, ξ can depend only on three dimensionless groups, namely x/d, Re_d, and We_d. Independent variation of these three groups was accomplished by independent variation of d, x, σ, and u_f.

2.3   Splattering and its relation to jet disturbances

Figure 2-4 shows the amount of splattering at different nozzle-target separations for several nozzle diameters and Reynolds numbers. Each solid line represents data for a narrow range of Weber numbers, varying by less than $\pm 3\%$ around the stated
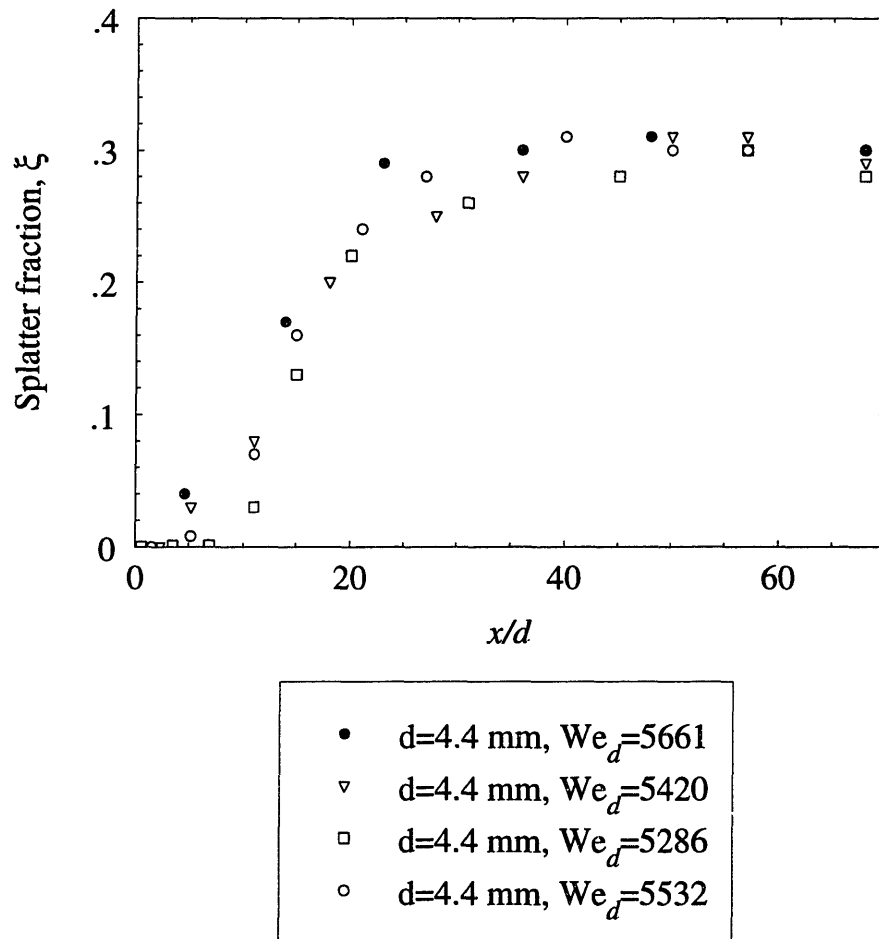
Figure 2-3: Scatter in the measurements of splatter fraction for water jets of nearly same Weber numbers.

mean value, a range equal to the experimental uncertainty of We_d. Splattering of as much as 75% of the incoming fluid is observed at a Weber number of 31,000 and a Reynolds number of 98,000 for a nozzle-target separation of $x/d = 34$.

At any given Weber number and nozzle-target separation, the splatter fraction, ξ, depends extremely weakly on the Reynolds number, if at all. For example, in the data set for $We_d = 5500$, the Reynolds number increases by a factor of 1.5 without any discernible change in the splatter fraction, ξ. In contrast, a factor of 1.3 increase in the Weber number (from 5500 to 7300) produces significant increase in the splatter fraction (roughly +25%).

An influence of Reynolds number would be expected to arise primarily from viscous effects near solid boundaries, either in setting the pipe turbulence-intensity or as an influence of the viscous boundary layer along the target. Past work (e.g. Lienhard et al. 1992) has established that the stagnation-point boundary layer is extremely thin relative to the liquid layer, and it thus may have little effect on the surface waves near the stagnation-point. To examine the effect of Reynolds number on turbulence intensity we refer to Laufer (1954). His measurements show the ratio of rms turbulent speed to friction velocity, u'/u_*, to be nearly independent of Reynolds number in fully-developed turbulent pipe-flows. Therefore

$$\frac{u'}{u_f} \propto \frac{u_*}{u_f} \propto \sqrt{f} \propto \mathrm{Re}_d^{-1/8}$$

where we have used the definition of $u_*(= u_f\sqrt{f/8})$ and the Blasius friction factor equation ($f = 0.316\mathrm{Re}_d^{-1/4}$ for $4000 < \mathrm{Re}_d < 10^5$). This weak dependence of the turbulence intensity on the Reynolds number may be the reason that we observe no significant dependence of splattering on the jet Reynolds number over the present range of Re_d.

Splattering of some small diameter, long jets are shown in Figure 2-5. These jets splatter less than 10% of the incoming flow for nozzle-target separation, x/d below 110. This splatter fraction is less that that for the jets in Figure 2-4 over the same range of nozzle-target separations. This is consistent since these small
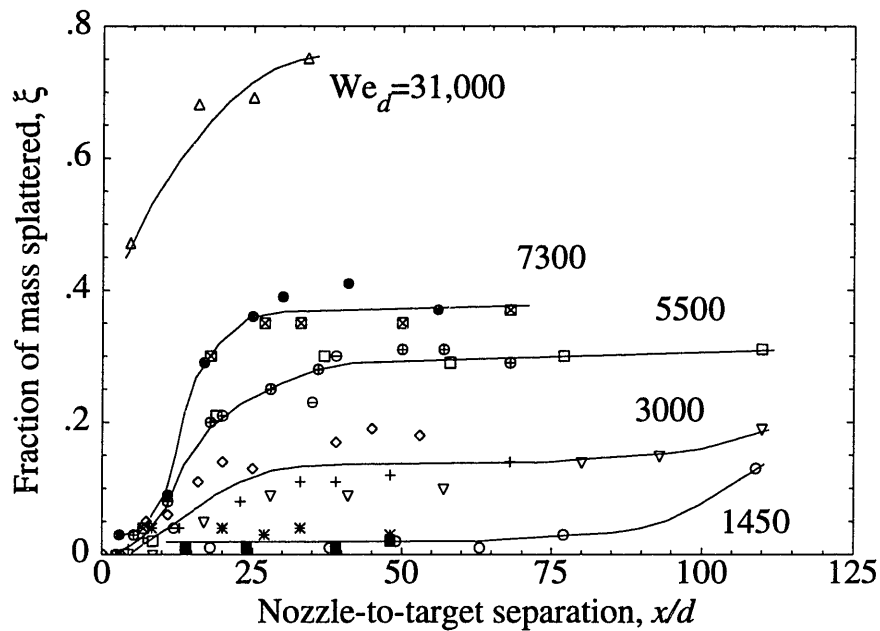
△	d=4.4 mm, Re_d=98097, We_d=31243
⊠	d=4.4 mm, Re_d=48284, We_d=7564
●	d=2.7 mm, Re_d=37141, We_d=7096
⊖	d=5.8 mm, Re_d=47800, We_d=5628
⊕	d=4.4 mm, Re_d=41437, We_d=5420
□	d=2.7 mm, Re_d=31868, We_d=5373
◇	d=5.8 mm, Re_d=35986, We_d=3101
+	d=4.4 mm, Re_d=30090, We_d=2858
▽	d=2.7 mm, Re_d=24580, We_d=3108
✳	d=5.8 mm, Re_d=24507, We_d=1479
■	d=4.4 mm, Re_d=20988, We_d=1430
○	d=2.7 mm, Re_d=16320, We_d=1409

Figure 2-4: Splattering as a function of nozzle-target separation and jet Weber number. Solid lines are fitted curves for Weber number constant to within ±3% (which is the uncertainty of experimental We_d): We_d = 1450 (1409, 1430, 1479); 3000 (3108, 2858, 3101); 5500 (5373, 5420, 5628); 7300 (7096, 7564); 31000 (31243).

0.4

Plain water, d = 0.84 mm

Re$_d$ We$_d$

o   7003 836
+   5453 507
x   2765 130

0.35

0.3

0.25

ξ 0.2

0.15

0.1

0.05

0

0   100   200   300   400   500

x/d
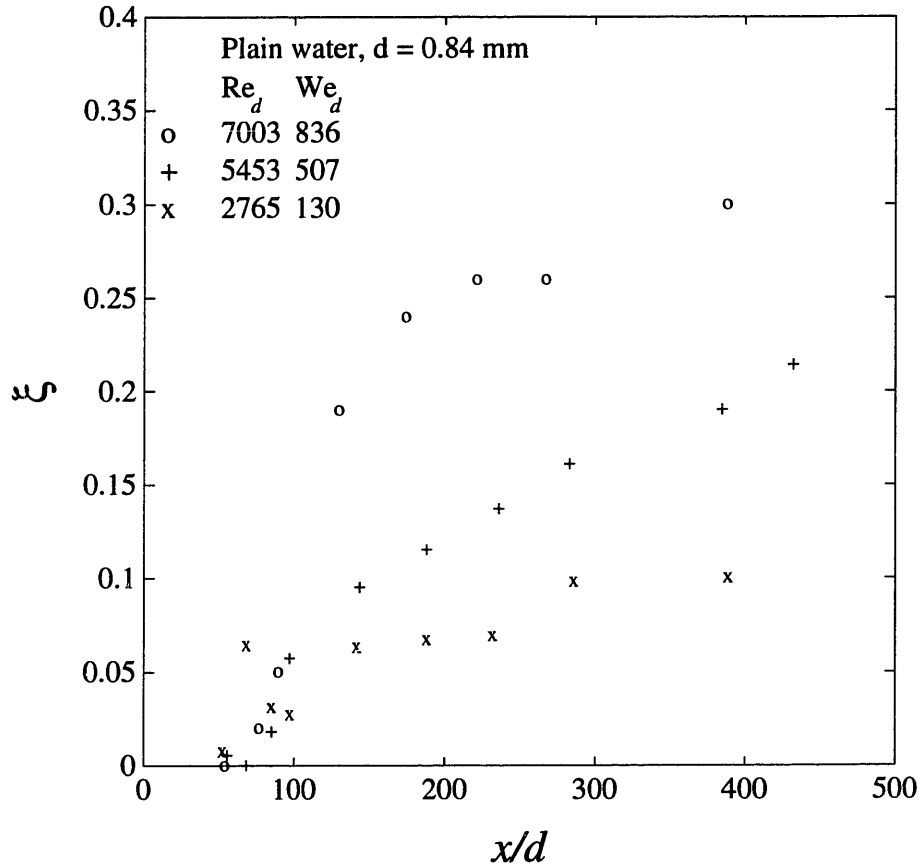
Figure 2-5: Splattering of small diameter, long jets.

diameter jets in Figure 2-5 have jet Weber number smaller than those in Figure 2-4. Here, as the nozzle-target separation increases the splattering increases towards an asymptotic limit, the actual limiting value depending on the jet Weber number. It is also noteworthy, that for such small diameter jets over an initial length of it, $x/d < 50$ or so, there is no measureble amount of splattering.

To study the effect of surface tension variation on splattering, a solution of approximately 10% by volume of isopropanol in water was used. The surface tension of the solution was measured before each run of the experiment; it was thus maintained at 0.042 N/m within ±5% accuracy (versus 0.072 N/m for pure water). Density was also measured. The data show (Figures 2-6, 2-7, 2-8) that the splatter fraction, ξ, still scales with Weber number, We$_d$, as observed before for the water jets. The splatter

fraction data for water and for an isopropanol-water solution, at a given jet Weber number, agree to within the experimental uncertainty in all but one case (Figure 2-7, $We_d = 5368$).

Referring to Figures 2-4 to 2-8, we see that very little splattering occurs close to the jet exit (small x/d), typically less than 5%. Beyond this region, the amount of splattering at first increases with distance, x/d. Farther downstream, it reaches a plateau. To explain these observations we refer to some measurements of the amplitude of turbulent liquid jet surface disturbances to be described in Chapter 3. The rms amplitude of jet surface disturbances at different axial locations of the jet, were obtained from the measurements of the instantaneous disturbance amplitude, using a non-intrusive, optical instrument. Starting from nearly zero near the nozzle exit, the rms amplitude of jet surface disturbances initially grows rapidly as the jet moves downstream; farther downstream the growth rate diminishes and the rms disturbance tends to an asymptotic limit. This growth of disturbances is the probable cause of the increase in the splatter fraction as the jet moves downstream. The steadily decreasing rate of amplitude growth results in a plateau of the disturbance amplitude which corresponds to that in the splatter fraction data.

For very long, low Weber number jets the plateau of splattering ends and ξ again increases with x/d (Figure 2-6, $We_d = 1450$). This may reflect the appearance of ordinary capillary instability on these jets. Specifically, when the Weber number is low, the asymptotic turbulence-generated surface roughness is small compared to the jet radius. Thus, the still nearly-cylindrical jet can give up surface energy by the usual Rayleigh-type instability. These observations are consistent with the data in Figure 2-5, where the jet Weber numbers being very low, turbulent surface disturbances are too small to cause any splattering near the nozzle. They start to casue splattering when they are long enough to have developed Rayleigh-type capillary disturbances. In contrast, at higher Weber number the turbulent disturbances grow to be as large as the jet radius, effectively breaking up the jet. In the low Weber number case, the splattering plateau ends when capillary instability further raises the jet roughness. In the high Weber number case, the plateau is reached when the jet is essentially broken

Figure 2-6: The Weber number correlates the splatter fraction, ξ as the surface tension of the jet fluid is varied (0.072 N/m for water & 0.042 N/m for isopropanol/water solution).

The figure shows a plot with "Fraction of mass splattered, ξ" on the y-axis (0 to .4) and "Nozzle-to-target separation, x/d" on the x-axis (0 to 80). Labeled "d = 4.4 mm".
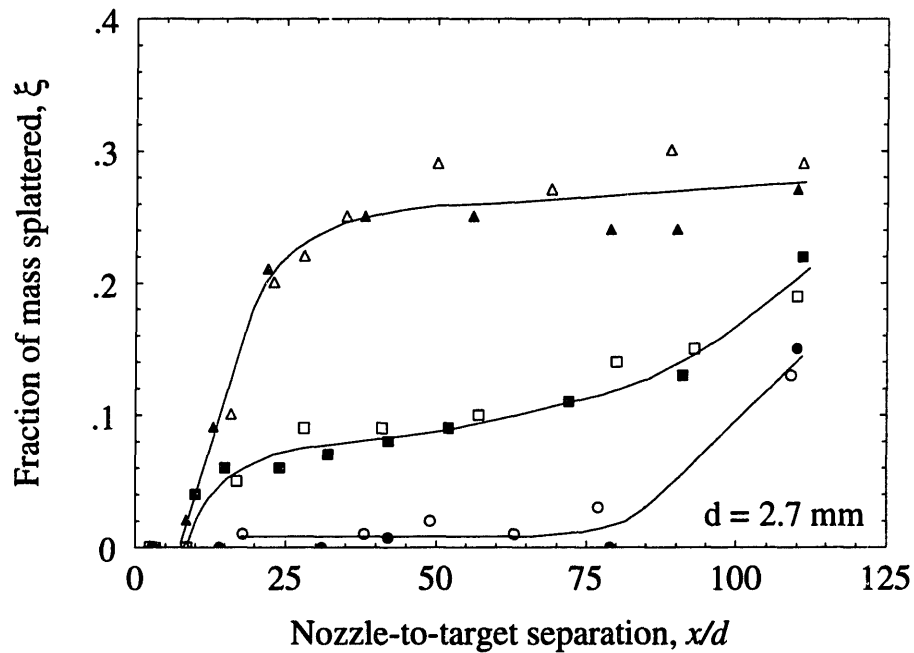
Legend:
▲ Isopropanol/water, We_d=7652
■ Isopropanol/water, We_d=5400
● Isopropanol/water, We_d=2806
△ Water, We_d=7564
□ Water, We_d=5400
○ Water, We_d=2858

Figure 2-7: The Weber number correlates the splatter fraction, ξ as the surface tension of the jet fluid is varied (0.072 N/m for water & 0.042 N/m for isopropanol/water solution).

Figure 2-8: The Weber number correlates the splatter fraction, ξ as the surface tension of the jet fluid is varied (0.072 N/m for water & 0.042 N/m for isopropanol/water solution).
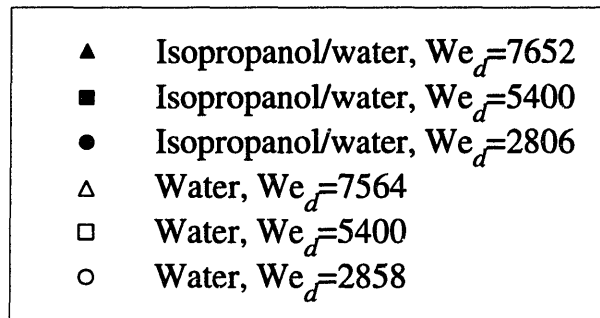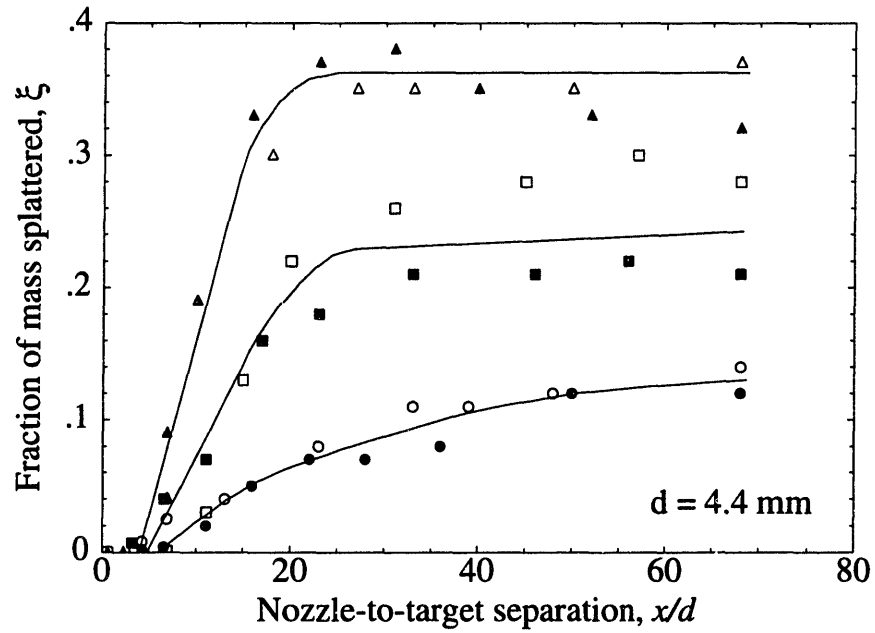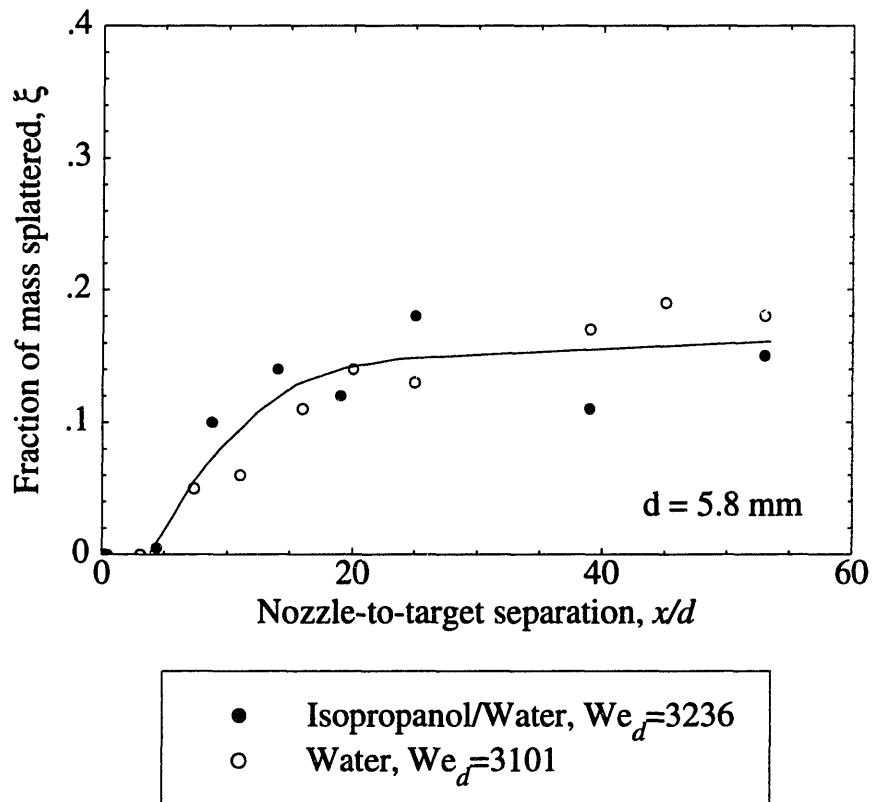
up into drops.

Once the jet is broken up, the splattering is effectively due to the impact of individual droplets. For a given Weber number, the size and velocity of those droplets remain nearly constant with increasing x/d (excluding the effect of air drag); thus the amount of splatter reaches an asymptotic value. Presumably, this asymptote depends on droplet Weber number (which is roughly equivalent to jet Weber number).

On the basis of the present experiments, we find that the range of applicability of the LLG model is $10^3 < \text{We}_d < 5 \times 10^3$, $x/d < 50$ and $4400 < \omega < 10,000$. Figure 2-9 shows both the present data and the LLG data in $\xi - \omega$ coordinates. The scaling with ω correlates the data reasonably well in this range. While LLG used nominal tube diameter in their data reductions, all data in Figure 2-9 are scaled with measured diameter. On this basis, we offer the following improved correlation for $\xi(\omega)$ in the range $4400 < \omega < 10,000$:

$$\xi = -0.258 + 7.85 \times 10^{-5}\omega - 2.51 \times 10^{-9}\omega^2 \tag{2.5}$$

The lower limit in terms of ω is chosen to ensure that the predicted ξ is at least 4%. Below this level there is considerable scatter and high uncertainty in the measurements.

For larger x/d or We_d, the ω model fails (Figure 2-10), but a different pattern emerges. For $\text{We}_d = $ constant, ω becomes a function of x/d only and we see curves similar to the ones in Figure 2-4.

2.3.1 The influence of surfactants

Surfactants lower liquid surface tension by forming a surface-adsorbed monolayer at the liquid surface. When a new liquid surface is formed, some time is required for surfactant molecules to diffuse to the surface in sufficient concentration to alter the surface tension. To study the role of surfactants in splattering, a mixture of approximately 0.2% detergent in water was used. This reduced the surface tension of the static solution (liquid surface at rest) to 0.027 N/m and corresponded to a
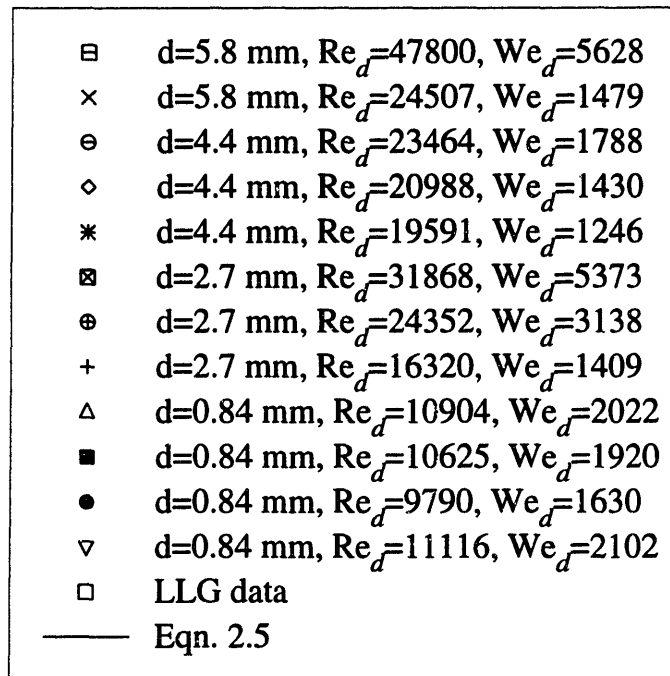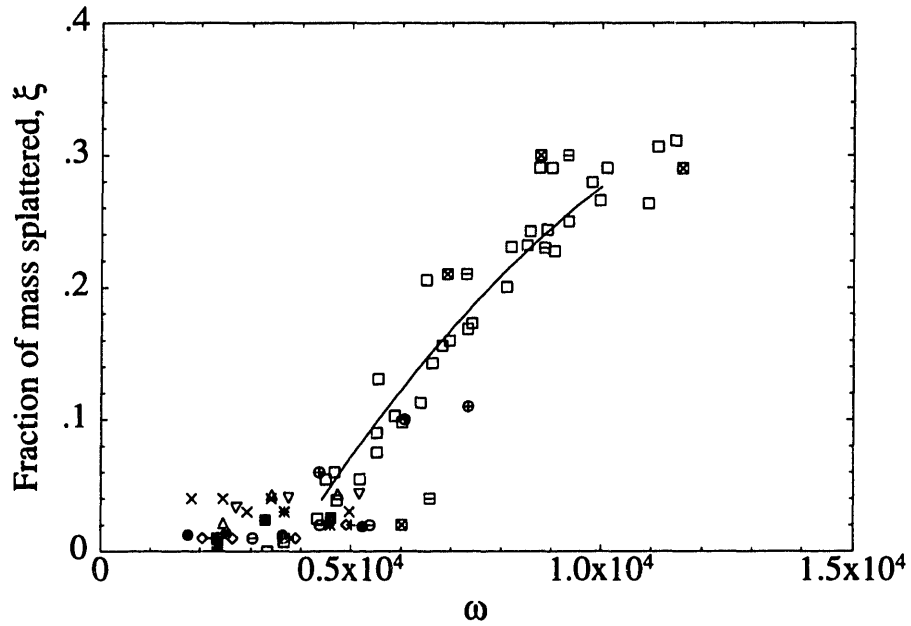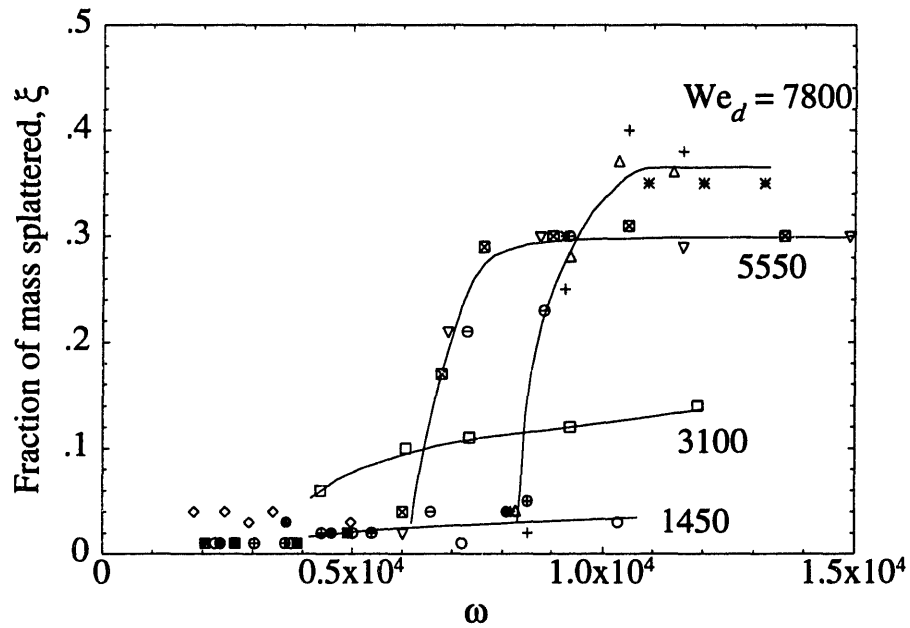
31

Figure 2-9: Comparison of the LLG model's scaling with the present data for $x/d < 50$.

Figure 2-10: Breakdown of the LLG model for $x/d > 50$ or $We_d > 5000$.

saturated surface concentration of surfactant. Figures 2-11 and 2-12 show that the presence of the surfactant does not alter the amount of splattering. The splatter fraction for the surfactant-laden jet is identical to that for a pure water jet of the same velocity, diameter and length; in fact, if the surfactant-jet Weber number is calculated on the basis of pure-water surface tension, the curves for the surfactant-jets are identical to those of the pure jets. From the standpoint of splattering, the surface tension of the surfactant-jet is effectively the surface tension of the pure liquid.

Possible reasons for this behavior are as follow. Inside the nozzle, the surfactant is in the bulk of the liquid. When the liquid exits the nozzle, a new free surface is formed which is not initially saturated with surfactant. Because a finite time is required for the surfactant to diffuse from the bulk to the free surface, the surface remains unsaturated over some initial length of the jet. In this initial region, the surface tension remains near that of pure water.

The time required for the surface concentration of surfactant to reach saturation was estimated for turbulent diffusion from the bulk to the free surface under the assumption that all surfactant reaching the surface is captured by and remains on the surface (Appendix A). Using Köhler's (1993) correlation for interphase mass transfer across free surface, this model yields an unsaturated length of only 3 to 4 diameters for the two cases in Figure 2-11. However, the model is unreasonable in that it neglects any turbulent reentrainment of surfactant from the surface to the bulk, an effect that is probably quite large. Thus it seems likely that the time required to achieve saturation is significantly longer, if saturation is reached at all. In consequence, only the surface tension of the bulk liquid appears to play a role in splattering, at least for the lengths of the jets in this study. The data show clearly that the presence of a surfactant does not alter the splattering characteristics.

To help resolve this issue, measurements of the jet surface roughness evolution with surfactants has been compared to those without any surfactant (Section 3.3.2). These preliminary measurements indicate that the presence of surfactants do not alter the rms amplitude of turbulent disturbances on jet surface. As a result the amount of splattering is not influenced by the presence of a surfactant in the jet liquid.
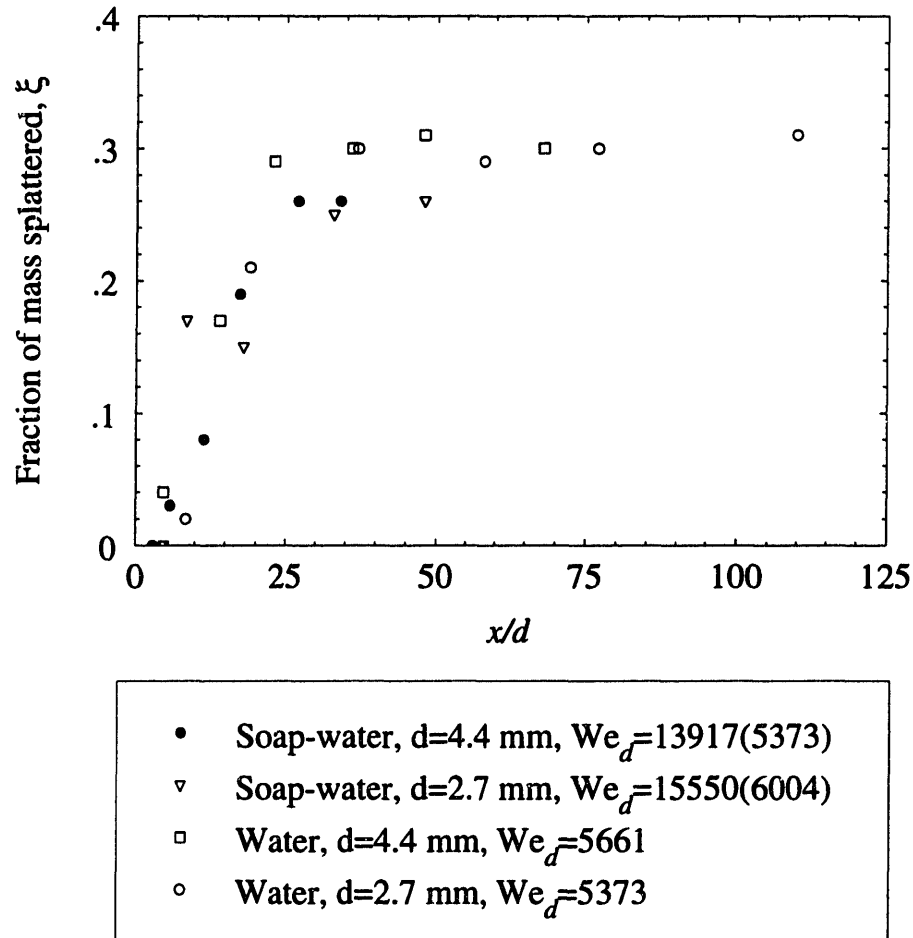
Figure 2-11: No effect of surfactants on splattering. The Weber numbers of the soap-water jets are based on the surface tension of the surfactant-saturated surface. The Weber number in parenthesis is based on the surface tension of pure water.

0.35

0.3

0.25

0.2

ζ

0.15

σ (N/m) Re$_d$ We$_d$
o Soap-water 0.027 6871 2000(767)
x Plain water 0.072 7003 836
d = 0.84 mm

0.1

0.05

0

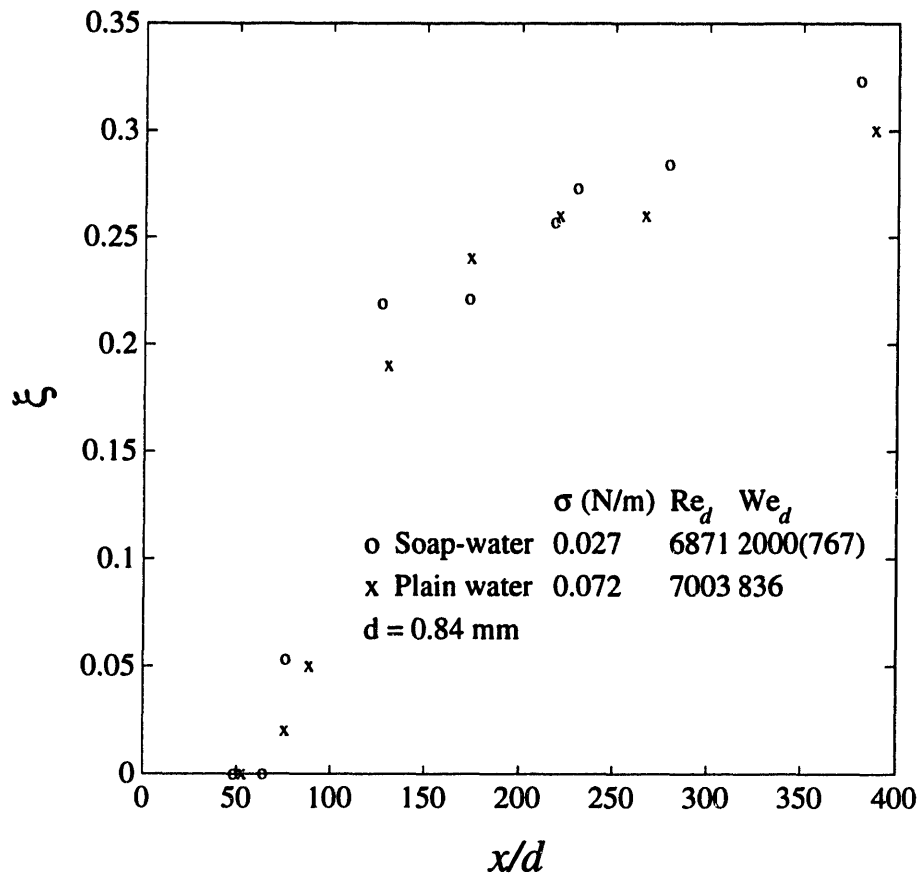0   50   100 150 200 250 300 350 400

x/d

Figure 2-12: No effect of surfactants on splattering even for very long jets. The Weber number of the soap-water jet is based on the surface tension of the surfactant-saturated surface. The Weber number in parenthesis is based on the surface tension of pure water.

Formation of bubbles is a possible source of error in the measurements of splatter fraction and the amplitude of surface disturbances (Section 3.3.2), with jets of low surface tension liquids, especially with detergents. To minimize bubble formation test were done in short intervals with long delay between runs for bubbles to float to free surface keeping the bulk of the liquid relatively bubble free.

2.3.2   The role of additives

Errico (1986) reported reduction in jet impingement splattering by adding very small quantities of a poly-electrolyte, Separan AP-273 to plain water. To see the effect of an additive, measurements of splattering was made with a solution of 500 weight-parts-per-million (wppm) of guar in water. Guar is a commonly used drag reducing agent in turbulent pipe flows. The surface tension of this guar solution was measured to be 0.052 N/m. Measurements show an increase in splattering over plain water jets of the same jet Weber number. This may appear contradictory to Errico's (1986) conclusions. First we note the very limited number of measurements with the additives in the present study. Also this may indicate that different additives do not influence splattering the same way.

2.3.3   The onset of splattering

Some problems arise in defining the onset point of splattering. Since the process of splattering involves turbulent flow, sporadic splattering of droplets occurs at much lower jet velocities than those that would cause any significant amount of sustained splattering (other parameters remaining the same). Consequently, the onset point is more accurately definable in terms of a non-zero level of splattering. Owing to the finite accuracy of measurement systems, this threshold should not be so low as to have substantial uncertainty. We chose to define the onset of splattering as the point where 5% of the incoming fluid is splattered. In view of our earlier observation that, for a given x/d, the amount of splattering depends strongly on the jet Weber number and not on the Reynolds number, we expect the onset point to be uniquely
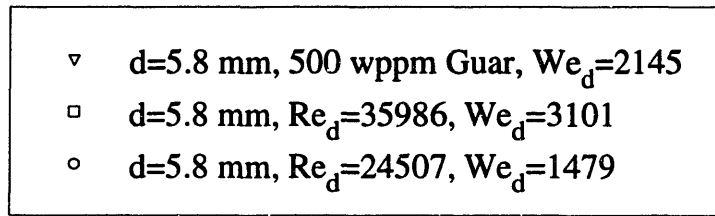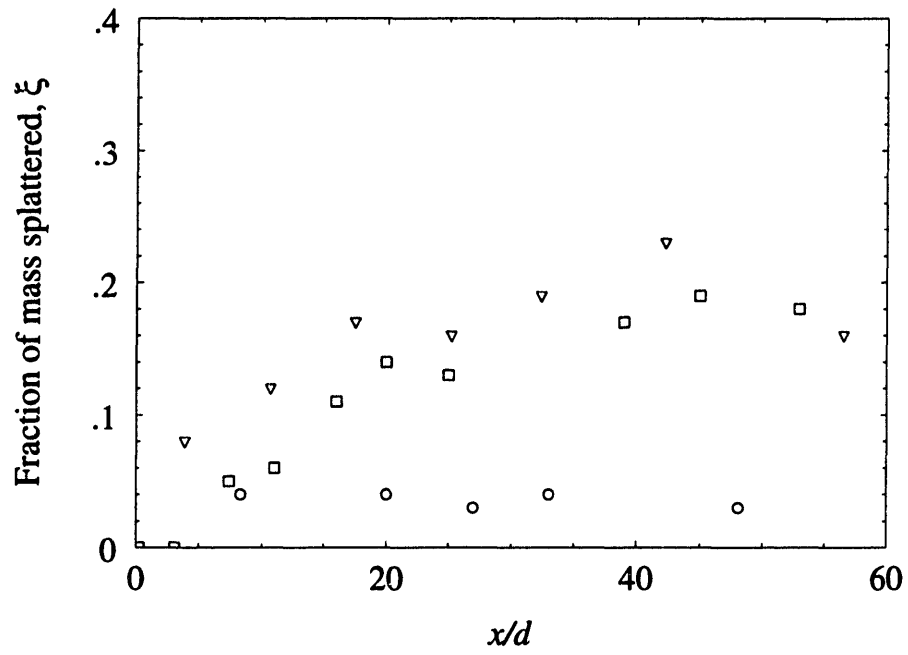
Figure 2-13: Comparison of splattering of jets of 500 wppm guar in water and plain water

identifiable by its x/d and We_d. In other words, for a jet of a given Weber number, the onset point is reached at a certain x/d.

Figure 2-14 shows the data for onset points. A correlation for the onset point data is

$$\frac{l_o}{d} = \frac{130}{1 + 5 \times 10^{-7}\,\mathrm{We}_d^2} \qquad (2.6)$$

For low Weber numbers, where surface tension dominates, comparison to the capillary breakup length is appropriate. When aerodynamic forces are negligible, the capillary breakup length of a uniform-velocity viscous jet is given by (Weber, 1931)

$$\frac{l_b}{d} = 12\sqrt{\mathrm{We}_d}\left(1 + \frac{3\sqrt{\mathrm{We}_d}}{\mathrm{Re}_d}\right) \qquad (2.7)$$

For the turbulent jets in this study, produced by a fully-developed turbulent pipe-flow, Re_d exceeds 2000. In such jets, when $\mathrm{We}_d \sim 100$ we find $l_b/d \sim 120$. Thus, the observed onset points at low Weber numbers are close to the capillary breakup point. In this range, splattering is essentially of drop impingement type. Apparently, turbulent disturbances are strongly damped by surface tension in these low Weber number jets, and capillary instability is dominant.

The relative importance of turbulence and surface tension is characterized by a balance of rms turbulent dynamic pressure and the capillary pressure. Thus, the appropriate Weber number for characterizing splattering mechanism is based on the rms fluctuating component of the velocity, u', and the rms height of the surface disturbances, δ_{rms}:

$$\widehat{\mathrm{We}} = \frac{\text{turbulent dynamic pressure}}{\text{capillary pressure}} = \frac{\rho u'^2}{\sigma/\delta_{rms}} = \frac{\rho u'^2 \delta_{rms}}{\sigma} \qquad (2.8)$$

$\widehat{\mathrm{We}}$ should be $\mathcal{O}(1)$ or greater when turbulence drives splattering. However, u' and δ_{rms} are not easily available, while u_f and d are, so we have used

$$\mathrm{We}_d = \frac{\rho u_f^2 d}{\sigma} = \widehat{\mathrm{We}}\bigg/\left[\frac{\delta_{rms}}{d}\left(\frac{u'}{u_f}\right)^2\right] \gg 1 \qquad (2.9)$$
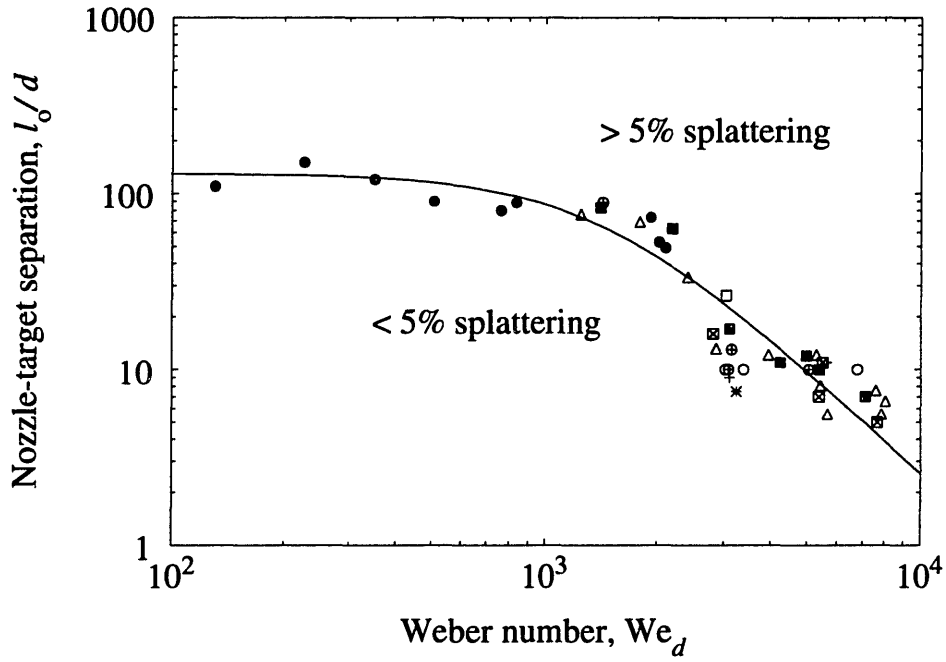
39

Figure 2-14: Onset of splattering.

which is 100–1000 times larger than the Weber number, $\widehat{We}$, that actually character-
izes physical processes involved here (since u'/u_f is a few percent in magnitude and
$\delta_{rms}/d < 0.5$).

The only other quantitative data on onset in literature — LLG and Womac et
al. (1990) — compare very well with the present study. Some data in the text and in
an accompanying figure in the paper by Womac et al. were combined to obtain the
onset points for their study. Apparently, they identified the onset points by visual
observations. This is likely to provide slightly different l_o/d than by our method.
Also, the visual determination of onset point depends on the size of the splattered
droplets and their optical properties, which in turn introduce additional uncertainties.
These factors may account for the slight discrepancies between their results and ours.

Stevens and Webb (1989) did not report any splattering for their turbulent jets.
The most likely reason for this is that, in their study, x/d was almost always smaller
than l_o/d. Only two of their reported data points lie within our splattering region
(specifically, $Re_d = 5 \times 10^4, d = 5.8$ mm, $x/d = 12.8$, $We_d \simeq 6.2 \times 10^3$ and $Re_d =
4 \times 10^4, d = 4.1$ mm, $x/d = 18.5$, $We_d \simeq 5.6 \times 10^3$).

LLG reported an onset criterion of $\omega \geq 2120$ for the appearance of *any* splattering.
In contrast, the present data show onset of any splattering over a range of values of
ω, $2000 < \omega < 8000$. Within the range of applicability of the LLG model which was
mentioned above, the onset of 5% splattering occurred for ω between 4100 and 5100.

2.3.4 The upper limit of splattering for high Weber number jets

As previously explained, the upper limit of splattering for high Weber number
jets should be reached near the breakup length of the jet. The breakup length of tur-
bulent jets is known to depend on Reynolds and Weber numbers (Lienhard and Day,
1970). Miesse (1955) reported correlations for breakup lengths, l_b, of turbulent liquid
jets subject to strong aerodynamic forces. From the data on jets from industrially-
used converging-orifice type nozzles in a Reynolds number range similar to ours, he

We_d	Re_d	l_c/d	l_b/d	l_b/l_c
5373	31868	25	61	2.44
5661	41757	24	53	2.2
7564	48284	20	56	2.8
8043	49770	18	56	3.1

Table 2.1: Comparison of observed upper-limit lengths to predicted capillary/aerodynamic breakup lengths of Miesse (1955).

reported

$$\frac{l_b}{d} = 540\sqrt{\mathrm{We}_d}\,\mathrm{Re}_d^{-5/8} \qquad (2.10)$$

The jets in the present study were produced by tube nozzles with fully-developed turbulent flow, so their breakup lengths can be predicted only in order of magnitude by this correlation. Table 2.1 compares the breakup lengths predicted by this correlation to the nozzle-target separations, l_c, at which the asymptotic upper limit of splattering is reached.

The predicted breakup lengths l_b are larger than the upper limit lengths l_c roughly by a factor of 2.6. This may be because this correlation overestimates the breakup lengths for the different nozzle geometry involved here. Alternatively, it may be that the splattering mechanism changes from jet impingement splattering to drop impingement splattering somewhat before the jet breakup location. In either case, the comparison shows a consistent relation between the jet breakup length and the upper-limit length of splattering.

2.4   Conclusions

Splattering has been measured for turbulent liquid jets impacting solid targets. Data span the range $0.2 \leq x/d \leq 125$, $2700 \leq \mathrm{Re}_d \leq 98{,}000$ and $130 \leq \mathrm{We}_d \leq 31{,}000$. The present results have been compared to the previous studies and improved

correlations have been developed.

- For a turbulent jet the amount of splattering is governed by the level of surface disturbances present on the surface of the jet. This observation is similar to those for laminar jets with externally-imposed disturbances.

- Amount of splattering at a given nozzle-target separation depends principally on the jet Weber number.

- The presence of surfactants in the jet does not alter the amount of splattering. Only the surface tension of the bulk fluid plays a role in splattering.

- The model proposed by Lienhard et al. (1992) is applicable for $1000 < \text{We}_d < 5000$ and $x/d < 50$. An improved version of their correlation is $\xi = -0.258 + 7.85 \times 10^{-5}\omega - 2.51 \times 10^{-9}\omega^2$, for $4400 < \omega < 10{,}000$. Outside this range, We_d and x/d should be treated as independent parameters.

- The onset point of splattering for a 5% threshold is given by the correlation $l_o/d = 130/(1 + 5 \times 10^{-7}\,\text{We}_d^2)$.

- The upper-limit length of splattering, beyond which ξ is constant, appears to be related to the jet breakup length.

- Over the range of Reynolds numbers in this work, no significant effect of jet Reynolds number is identifiable. However, a very weak dependence on Reynolds number is likely to be present in all of the conclusions and the correlations presented in this study. Any extrapolation above $\text{Re}_d = 100{,}000$ should be done skeptically.

Chapter 3

Surface Disturbance Evolution on Turbulent Liquid Jets and its Relation to Splattering

3.1 Introduction

The disturbances on the free surface of an unsubmerged turbulent liquid jet control the splattering of an impinging jet. No detailed measurements of the instantaneous amplitudes of these disturbances are available in the present literature. Many photographic studies of turbulent liquid jets have been reported (Hoyt et al. 1974, for example). But the photographic technique is unsuitable for quantitative study of the time evolution of the amplitude of disturbances, since this would require an enormous number of photographs to achieve wavenumber decomposition. The only measurements of the amplitude of turbulent disturbances that the author found in the literature were by Chen and Davis (1964). They presented a few measurements using an electric conductivity probe. The accuracy of those measurements was severely limited by the interference of the instrument with the flow.

Here, we use a laser-based optical technique to measure the amplitudes of fluctuations on the free surface of a turbulent water jet in air (following Tadrist et al. 1991). This instrument, consisting of a laser light sheet, a photosensor, and lenses, is capable

of measuring fluctuations at frequencies up to about 1 MHz. Jets were produced by fully developed turbulent pipe flow issuing from tube nozzles. Measurements were made over the portion of the jet between 0.2 and 30 nozzle diameters in length. Data show a non-exponential growth of the rms amplitude of the surface disturbances on the jet as it moves downstream. Power spectra of the surface disturbances show that the turbulent disturbances dominate over the disturbances due to Rayleigh instability.

A mathematical model of free surface response to turbulence is also developed. At modest values of air-side Reynolds number, the free surface deforms in response to turbulent pressure fluctuations in the liquid. Capillary pressure provides the restoring force which balances the turbulent pressure, and this balance determines the amplitude and evolution of the free surface disturbances. Here, the high-wavenumber (small scale) portion of the turbulent pressure spectrum is modelled using results for homogeneous, isotropic turbulence. The balance of turbulent and capillary pressure is used to calculate the high-wavenumber spectrum of the surface disturbances. The theory shows the spectrum to decay as the -19/3 power of wavenumber, owing to the capillary damping of the turbulent pressure spectrum. This result is in good agreement with the measured spectra.

3.2   Experiments

A laser-based optical instrument (Figure 3-1) was used to measure the amplitudes of fluctuations on the free surface of a turbulent water jet in air. A similar instrument was used earlier by Tadrist et al. (1991) to measure the surface disturbances on laminar liquid jets. A He-Ne laser beam (2.4 mW) was transformed into a collimated sheet of light by sending it through a glass rod and a cylindrical lens (focal length, L = 44 mm) successively. This light sheet was further thinned and focussed onto the liquid jet by passing it through the axis of a cylindrical lens (L = 100 mm) such that an approximately 0.1 mm thick light sheet intersected the jet perpendicular to its axis. A collecting lens (L = 44 mm) focussed the portion of the light sheet unintercepted by the jet onto a photosensor. The photosensor was built based on an

EG & G Vactec photodiode (VTP 8552) for a dynamic range of about 1 MHz. A 5 V dc reverse bias was applied to the photodiode, reducing the junction capacitance to 44 pF. The vol tage drop across a resistor placed in series with the photodiode provided a signal corresponding to the amount of laser light power incident on it. Static calibration of the instrument, may be called a laser oscillometer, was done by placing metallic tubes of known diameters. It showed perfectly linear voltage variation of the measuring system with the width of the intercepted portion of the collimated laser sheet (Figure 3-2). The rms deviation from linearity was 1% of the full scale, i.e. of the voltage reading corresponding to the entire laser sheet. Precise measurements of the diameters of transparent glass rods by this instrument indicated the role of refractive index of the object to be negligible in these measurements; the glass rods (or water jets) act as diverging lenses making the intensity of the refracted light negligibly low some distance away from it, so that refracted light has no bearing on the measurements.

The output of the photosensor was analyzed by a digital oscilloscope (Hewlett Packard 54200 A/D) and a spectrum analyzer (GenRad 2512A). The oscilloscope provided the true rms voltages over portions of the signal. Several such rms voltage outputs were recorded to obtain the rms of the total voltage signal (AC+DC), V_{tot}, at a given jet axial location. The rms of the AC component of the signal, V_{ac}, was also recorded at each location. To measure the amplitude of fluctuations at one point on the jet surface, half of the width of the light sheet incident on the jet was obstructed by an optical mask so that only the fluctuations at one point on the jet surface contributed to the fluctuations in the amount of light received by the photosensor. $V_{1/2}$ denotes the rms of the corresponding AC signal. The voltage signal corresponding to the entire light sheet incident on the photosensor, without any interception, was noted as V_o. Owing to the linearity of photodetector response , the ratio of rms amplitude of surface fluctuations to the mean jet diameter, is simply

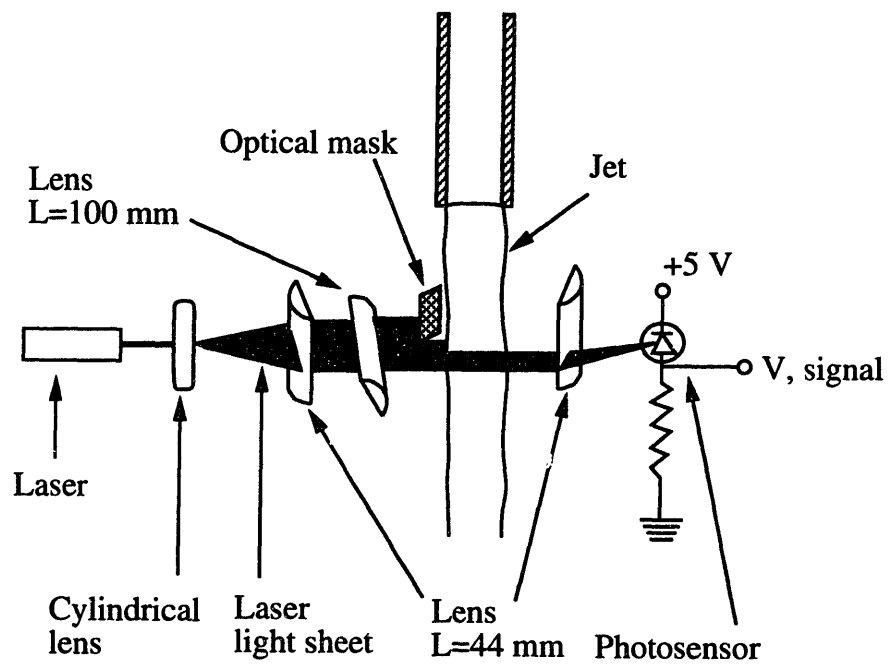$$\frac{\delta_{rms}}{d} = \frac{V_{1/2}}{V_o - \sqrt{V_{tot}^2 - V_{ac}^2}} \qquad (3.1)$$

Figure 3-1: Optical probe for the measurement of the instantaneous amplitude of jet surface disturbances.
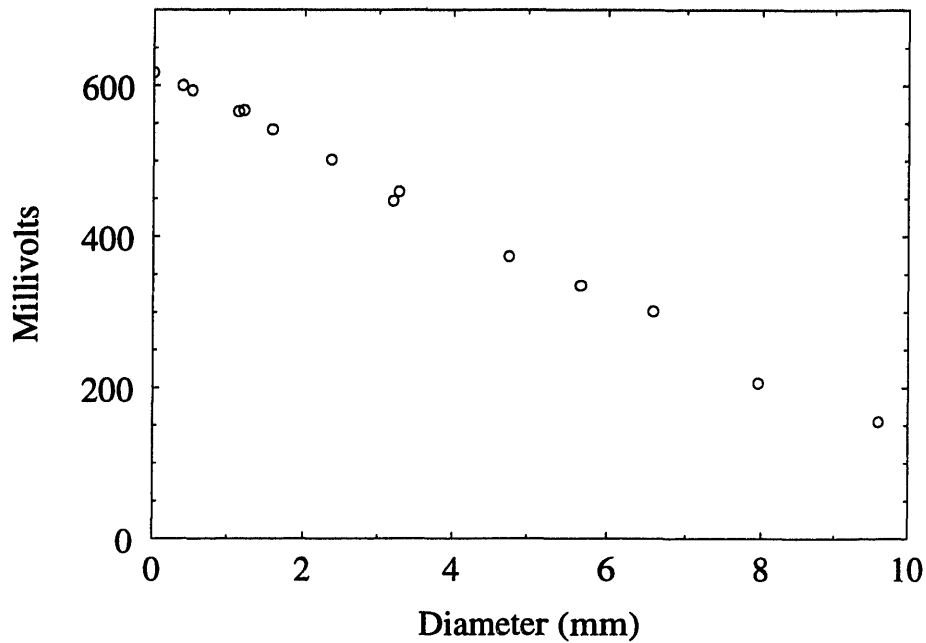
Figure 3-2: Calibration of the laser oscillometer.

The GenRad 2512A spectrum analyzer had a frequency bandwidth of dc to 100 kHz and an amplitude bandwidth of 6 decades for the power spectra.

The same apparatus as described in Chapter 2, was used for producing the jets. The jets emerged from tube nozzles of diameter d = 2.7 − 5.8 mm, with fully developed turbulent pipe flow upstream of the nozzle. Direct measurements of the flow rate provided the jet Weber numbers with ± 3% accuracy. As also observed in the splattering study, the jet Reynolds number has only a very weak role in the jets produced by fully developed turbulent pipe flows. Therefore, in this chapter the jet Reynolds numbers are not mentioned in the results presented though they can be easily calculated from the nozzle diameters and Weber numbers provided with each data set. The range of Reynolds number here is from 20,000 to 49,000.

Each measurement of δ_{rms} is based on an estimated number of 1000 samples. The actual number varied because of the sampling technique used in the oscilloscope; ten to twelve of the oscilloscope's values of $\overline{\delta^2}$ were averaged, each being based on oscilloscope samples of about 100 points. Some additional uncertainties can enter
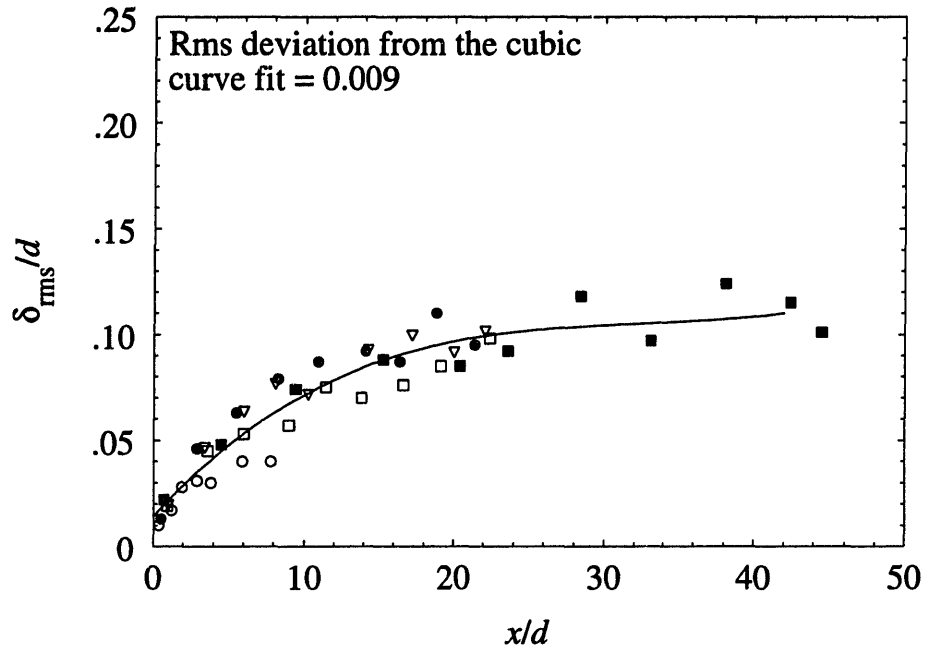
into the measurements when the jet Weber number and the length of the jet, x/d, became large enough so that droplets were stripped off the jet surface and entered the air flow around the jet. For the measurements reported here this droplet stripping was either absent or of negligibly low amount.

3.3 Measurements of surface disturbances

Figures 3-3 to 3-6 show the rms amplitudes of disturbances on turbulent water jets in air. To estimate the true run-to-run variability in the measurements, tests were repeated several times for nearly identical conditions (Figure 3-3). The jet Weber numbers for each test case were equal within the uncertainty limits of ±3%. The rms deviation of the measurements from the second order least-squares curve fit was 0.009 which was about 9% of the maximum amplitude of disturbance, δ_{rms}/d, for this test case. The 90% confidence intervals of the measurements according to a χ^2 (Chi-square) test of 1000 sample points were so small that they were nearly the size of the symbols plotted.

Figure 3-4 shows the fitted curves for repeated measurements of δ_{rms}/d at two different jet Weber numbers. Although the ranges of variability for the two data sets overlap, the averaged curves show a dependence of the growth of the amplitude of jet surface disturbances on the jet Weber number. This dependence is more pronounced in Figure 3-6, comparing data having a larger difference in jet Weber number. The amplitudes of disturbances are very small near the nozzle. As the liquid moves downstream the disturbances grow as the liquid free surface responds to the turbulent pressure fluctuations in the jet stream. The disturbance evolution does not follow the exponential growth with x/d that may be expected from Rayleigh's theory (Drazin and Reid, 1981; Lienhard et al., 1992). It can also be seen easily from the data that the disturbance growth rate parameter predicted by Rayleigh's theory, $\frac{x}{d}/\sqrt{We_d}$ cannot correlate the disturbance amplitude data for jets o f different diameters and Weber numbers. The jet Weber number correlates the variations of the amplitude of surface disturbances on jets of different diameters (Figure 3-7 and3-8).

Figure 3-3: Variability in the measurements of the amplitudes of disturbances for nearly equal jet Weber numbers.
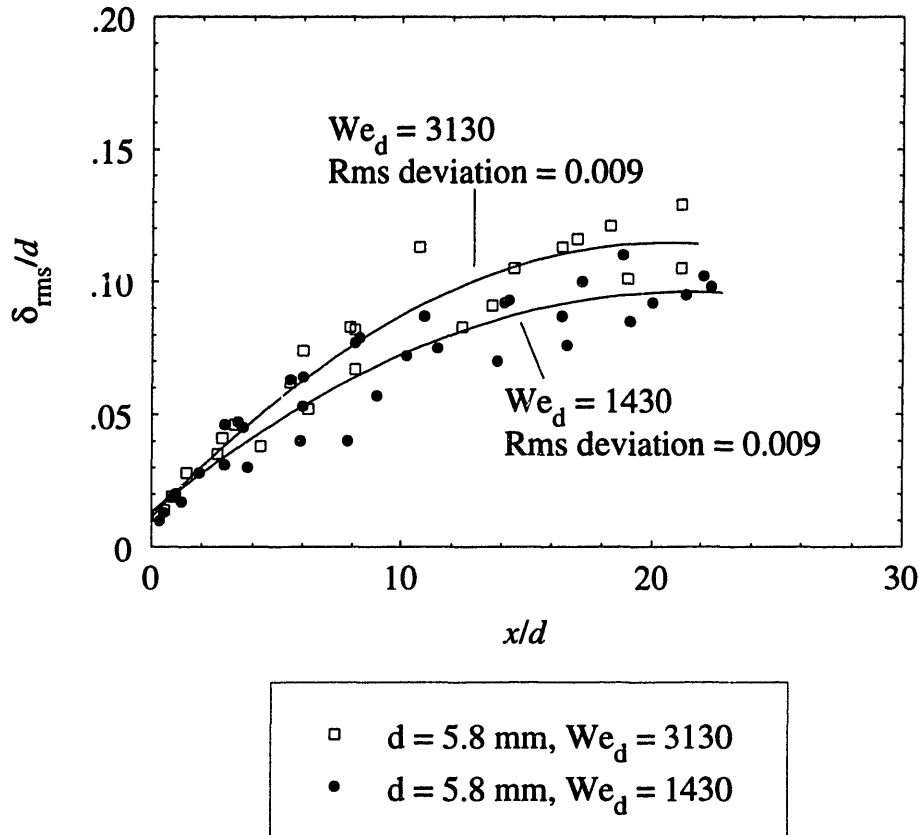
Figure 3-4: Scatter in the measurements of the amplitudes of disturbances at two different jet Weber numbers. For each Weber number, second order least-squares fitted curves and the rms deviation from the fitted curves are shown.

Figure 3-5: Measured amplitudes of surface disturbances on turbulent liquid jets.

Figure 3-6: Measured amplitudes of surface disturbances on turbulent liquid jets.

Figure 3-7: The jet Weber number correlates the variations of the amplitude of surface disturbances on jets of different diameters.

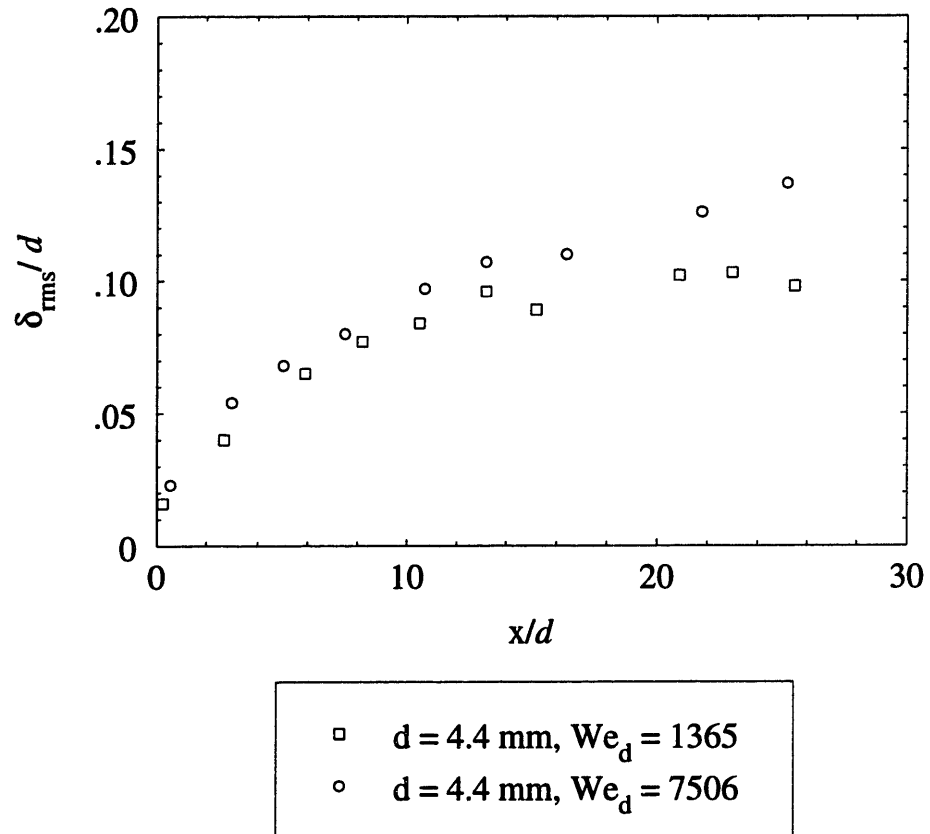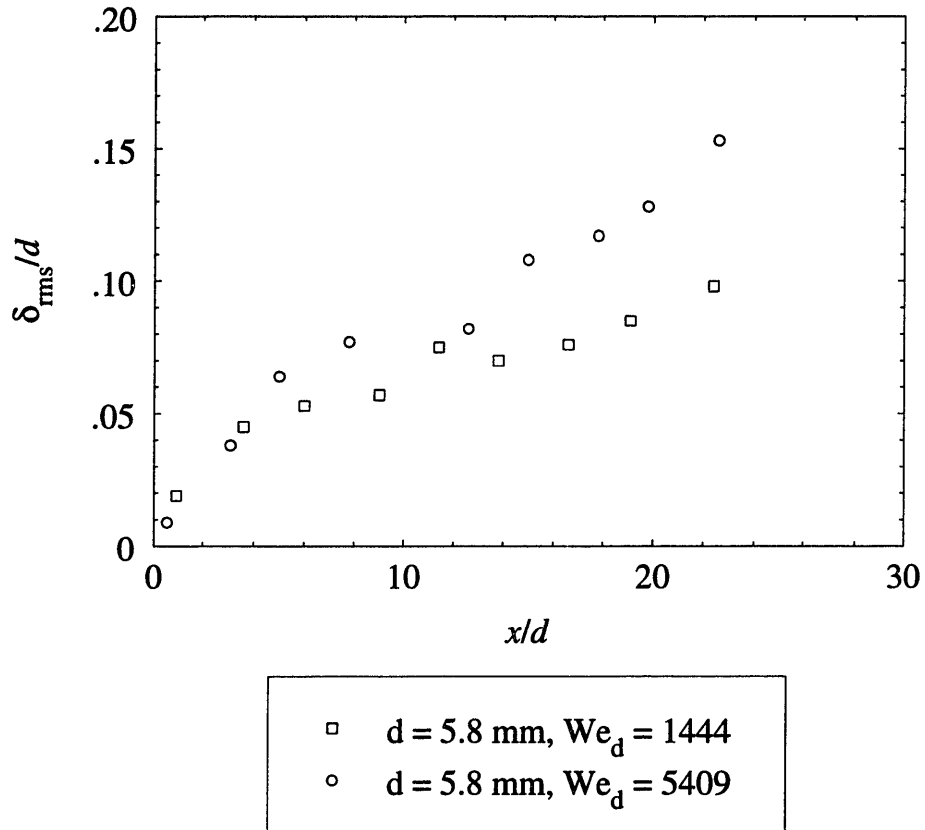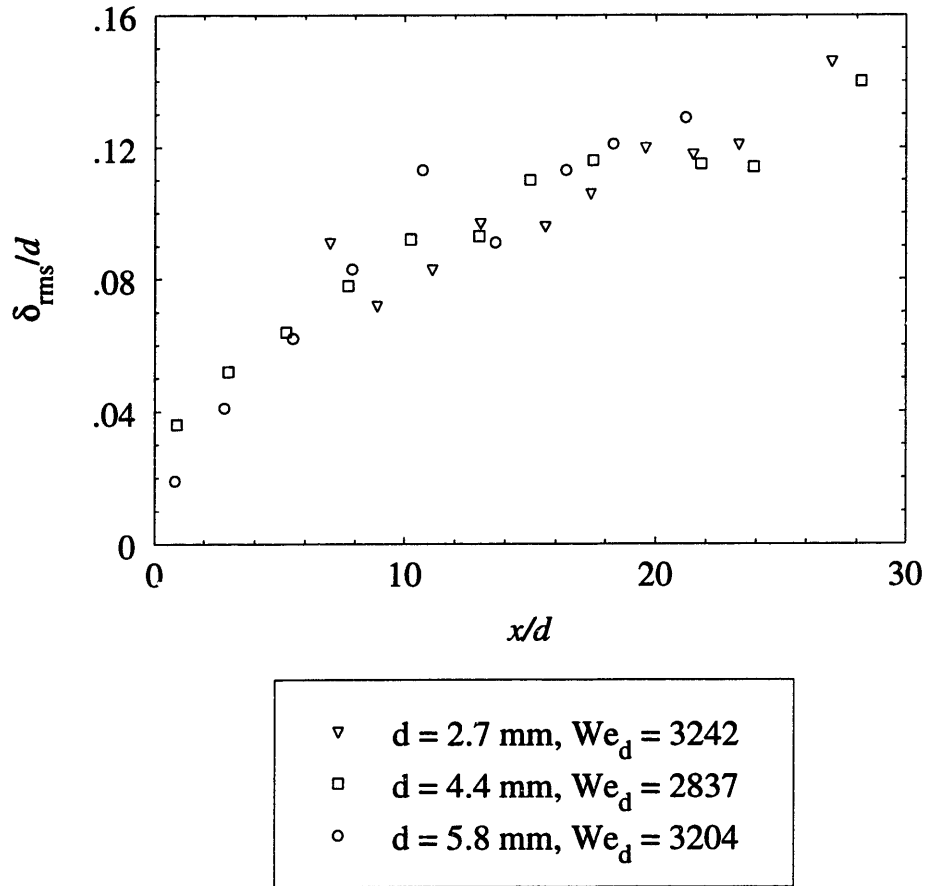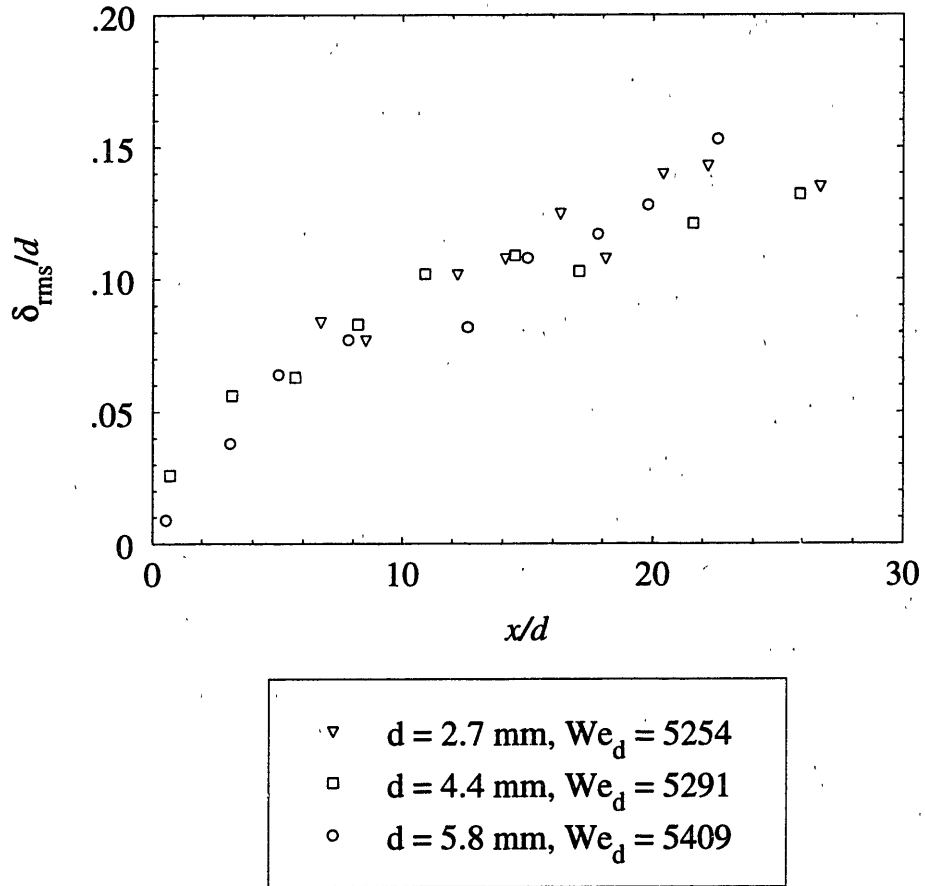Figure 3-8: The jet Weber number correlates the variations of the amplitude of surface disturbances on jets of different diameters.

We note the similarities between the variations of the amplitude of jet surface disturbances and the splatter fraction upon impingement as the jet moves downsteam (Figure 2-4). Near the nozzle ($x/d < 10$, say) there is very little change in ξ as the jet Weber number varies from 1400 to 7600. Similarly, the variation in δ_{rms}/d with the jet Weber number in Figures 3-4 to 3-6 is also very weak near the nozzle. Farther downstream, the dependence on jet Weber number is stronger both for δ_{rms}/d and ξ. These observations prompt us to investigate any possible correlation between the two quantitatively; such a correlation was the basic hypothesis of previous models of splattering (Lienhard et al., 1992).

Figure 3-9 shows a reasonably good correlation between the splatter fraction, ξ and the rms amplitude of jet surface disturbances. Each point on this graph is obtained by plotting previously measured splatter fraction ξ against δ_{rms}/d from present experiments for water jets of same Weber number and x/d. Each set of data for a given nozzle diameter and jet Weber number consists of measurements at several different axial locations, x/d. This provides further evidence that the jet impingement splattering is due to the presence of surface disturbances on turbulent jets and governed by the amplitudes of those disturbances.

Figures 3-10, 3-11 and 3-12 show the spectra of surface disturbances for different jets at several different axial locations. The ordinate is proportional to the power spectrum of the free surface disturbance amplitude, $G(k_1 l)$ (see Equation 3.8 below) and the abscissa is uk_1, where k_1 is the wavenumber in the direction of the jet axis, l is the integral scale of turbulence and u is the free surface velocity. For turbulent liquid jets, the free surface velocity reaches the average jet velocity within a couple of jet diameter lengths from the nozzle exit (Stevens and Webb, 1991). The spikes at very high frequencies are a reproducible noise signature of the electronics.

The log-log plots of the power spectra versus disturbance wavenumber show a portion of very nearly linear drop in the spectral amplitude, characteristic of high wavenumber turbulence. Except for the measurement locations very near the nozzle, the slope of this linear portion is -19/3. This is a consequence of the $k_1^{-7/3}$ variation of the one-dimensional spectrum of the pressure fluctuations (George et al., 1984)
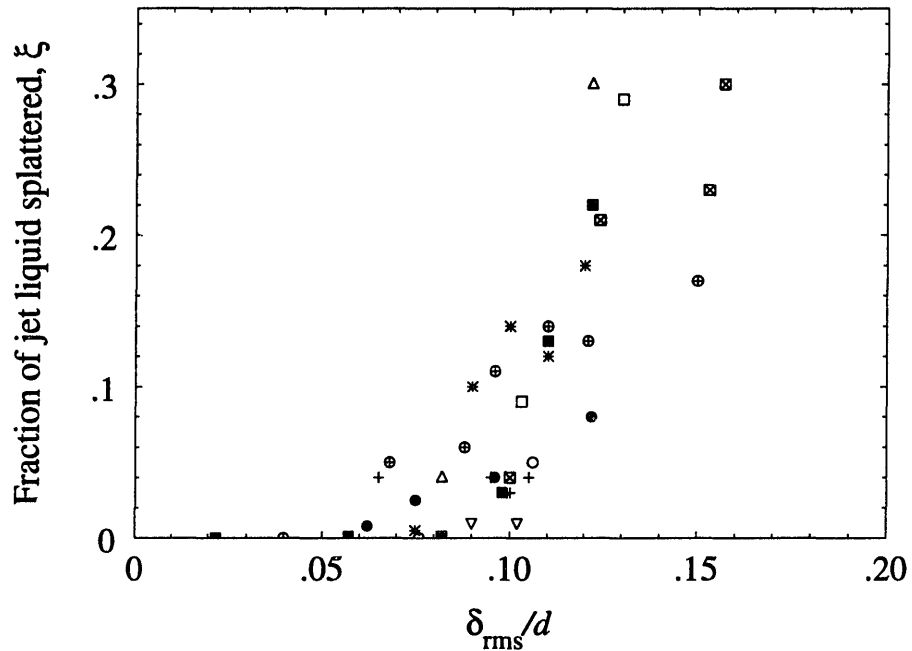
Figure 3-9: Correlation between the fraction of liquid splattered and the measured amplitude of jet surface disturbances.

Figure 3-10: Measured spectrum of turbulent liquid jet free surface disturbances. The ordinate is *proportional* to $G(k_1 l)$.
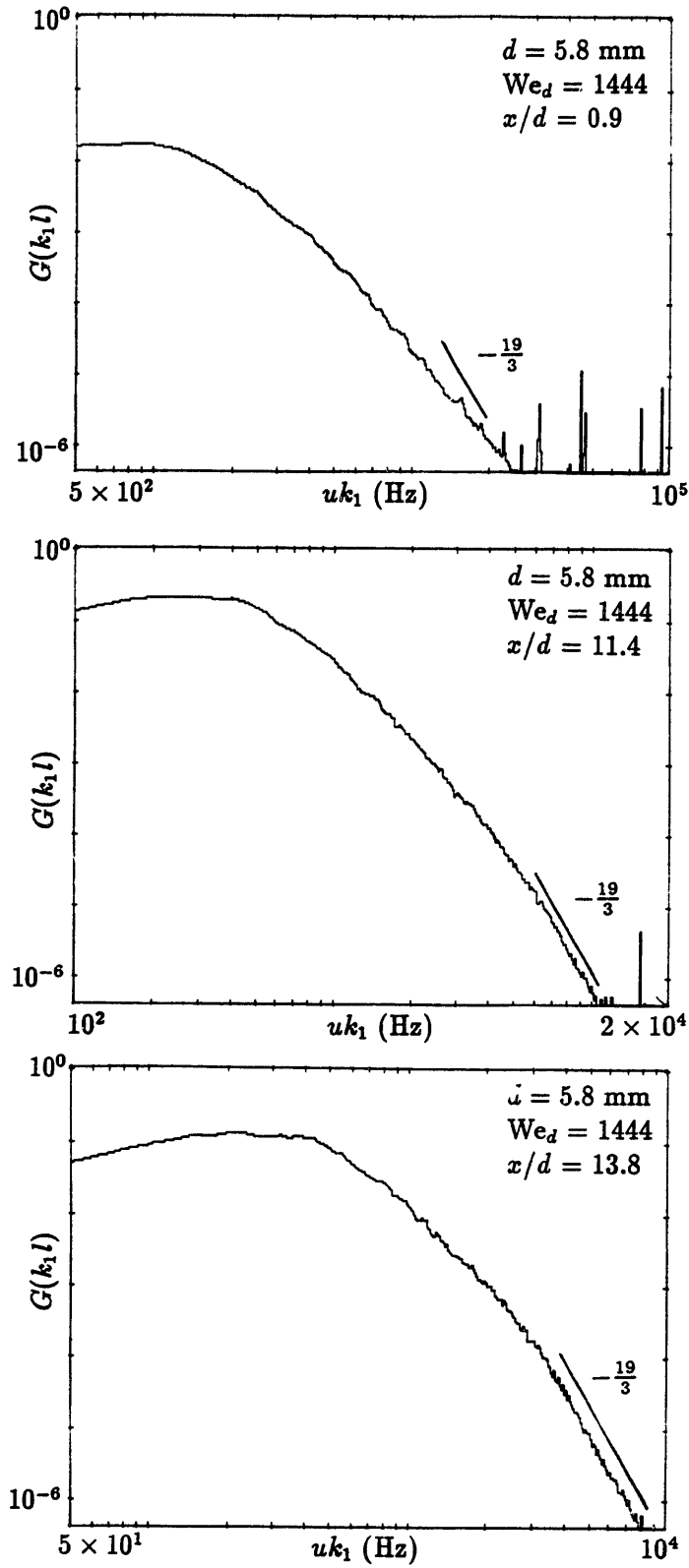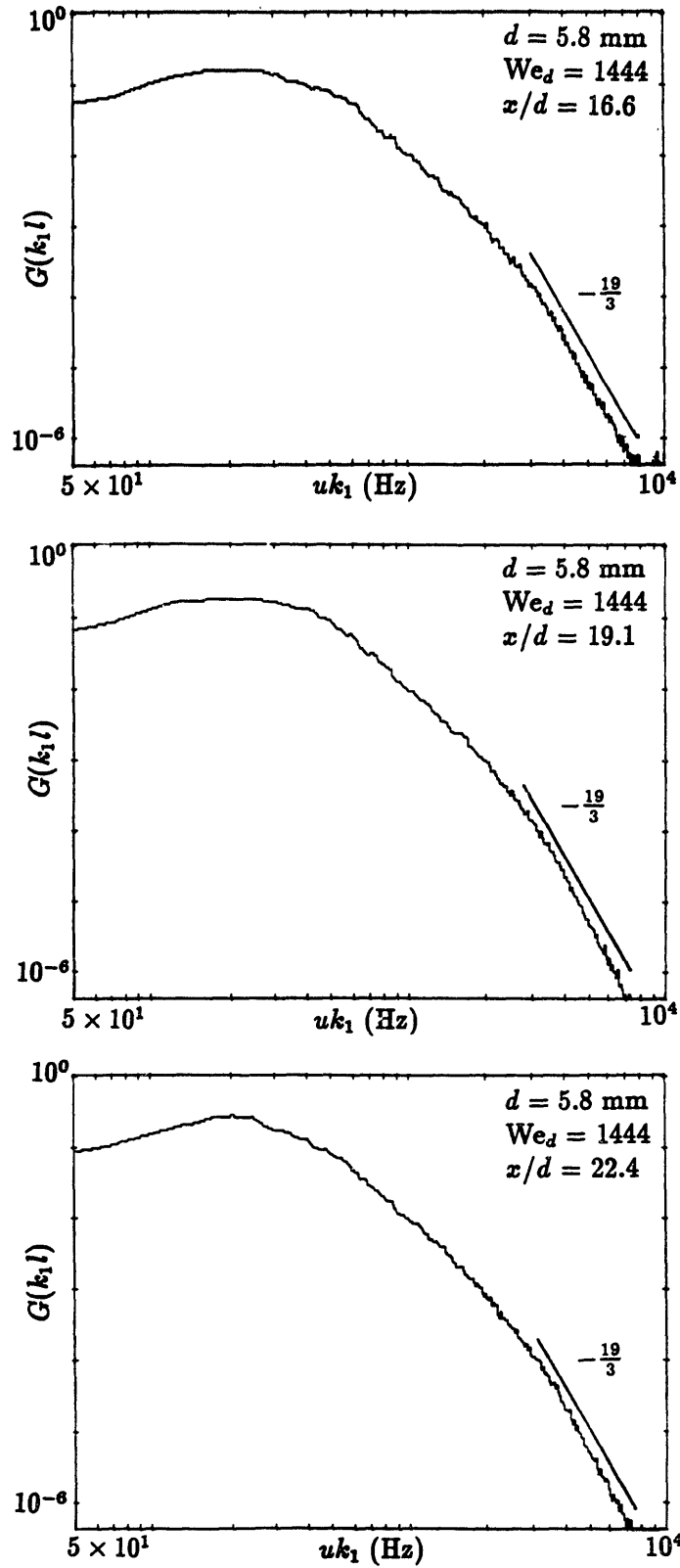
Figure 3-11: Measured spectrum of turbulent liquid jet free surface disturbances. The ordinate is *proportional* to $G(k_1 l)$.
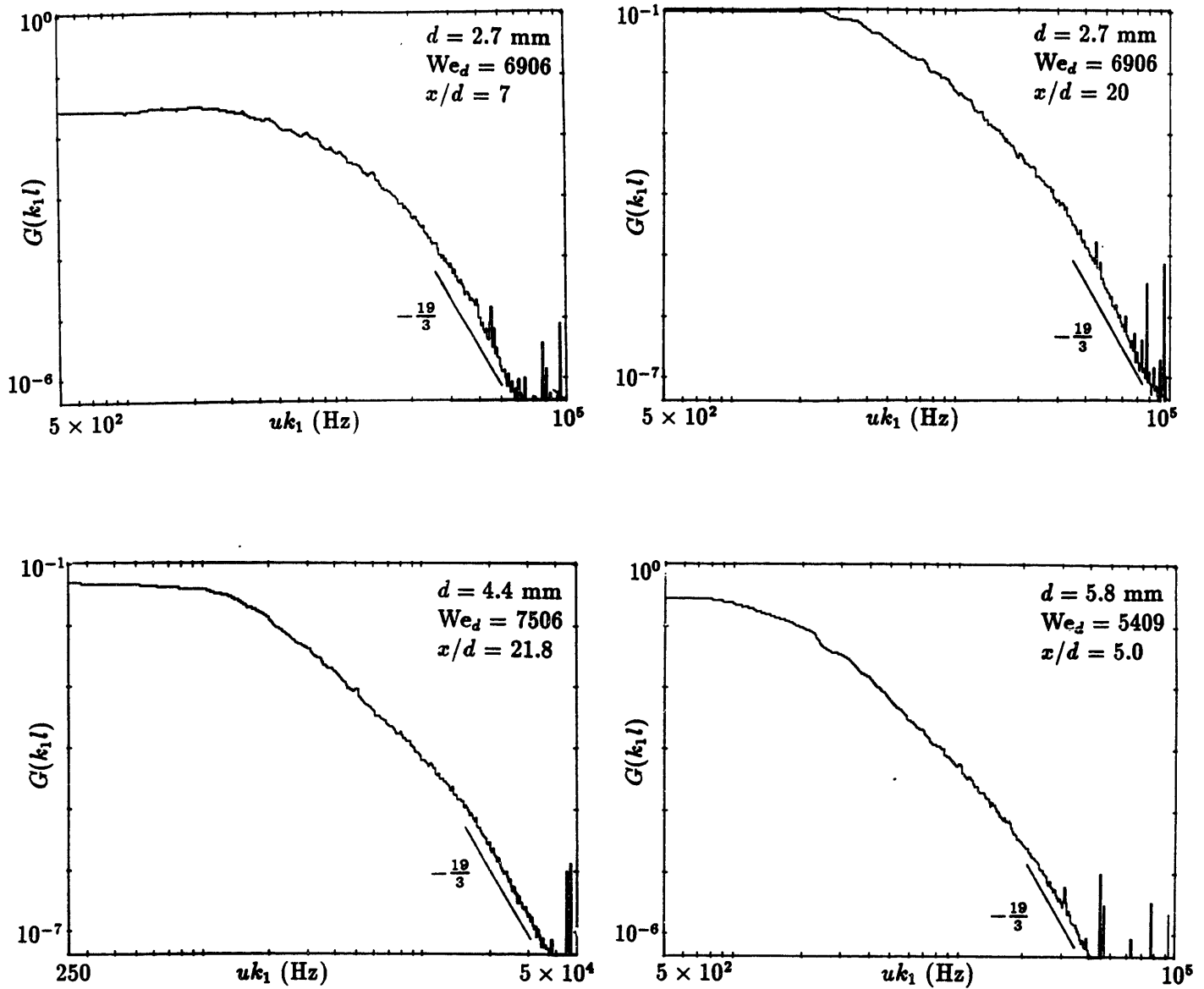
Figure 3-12: Measured spectrum of turbulent liquid jet free surface disturbances. Different nozzle diameters and jet Weber numbers than in previous figures. The ordinate is *proportional* to $G(k_1 l)$.

and the factor of k_1^{-4} introduced by the derivatives of δ involved in the capillary force balance equation (Equation 3.2 below). This is explained in detail in Section 3.4.

3.3.1 Variation of fluid properties

To study the effect of the variation of fluid properties, jets of approximately 10% by volume of isopropanol in water was used, as in splattering measurements. The surface tension of the solution was measured to be 0.042 N/m at room temperature (21 – 27 °C). A similar pattern of the growth of the amplitude of surface disturbances, as in water jets, is observed (Figure 3-13). Comparison of the data for isopropanol-water and pure water jets show that the jet Weber number correlates the variation of the amplitude of disturbances for different fluid systems (Figures 3-17 and 3-18).

3.3.2 The role of surfactants

To ascertain the role of surfactants present in a jet liquid, on the turbulent surface disturbance evolution, experiments were carried out with jets of water with detergent in it. As in the splattering study, approximately 0.2% by volume of a commonly available liquid soap was added to water. The measurements of the surface disturbance evolution on the jets of such mixtures are shown in Figures 3-14 through 3-16. The surface disturbance evolution on a surfactant-laden jet matches, within the scatter in the measurements, to that on a pure liquid jet of the same Weber number when the Weber number of the surfactant-jet is calculated based on the surface tension of the bulk liquid and *not* the surface tension of the surfactant-saturated surface. This confirms the observations of the lack of any effect of the surfactants on the general structure of a free-surface turbulent liquid jet by Hoyt et al. (1974) in their photographic study. Their photographs show no discernible effect due to th e presence of aerosol surfactants on water jets at various concentrations on the structure of the surface waves, location of the onset of droplet formation or the rate of droplet formation over an initial length of the jet of about 30 nozzle diameters.
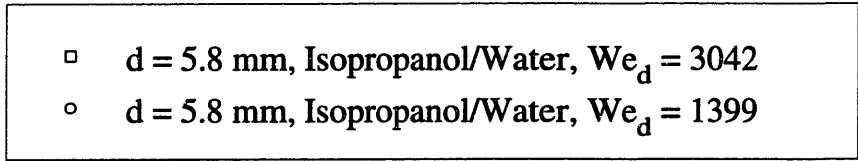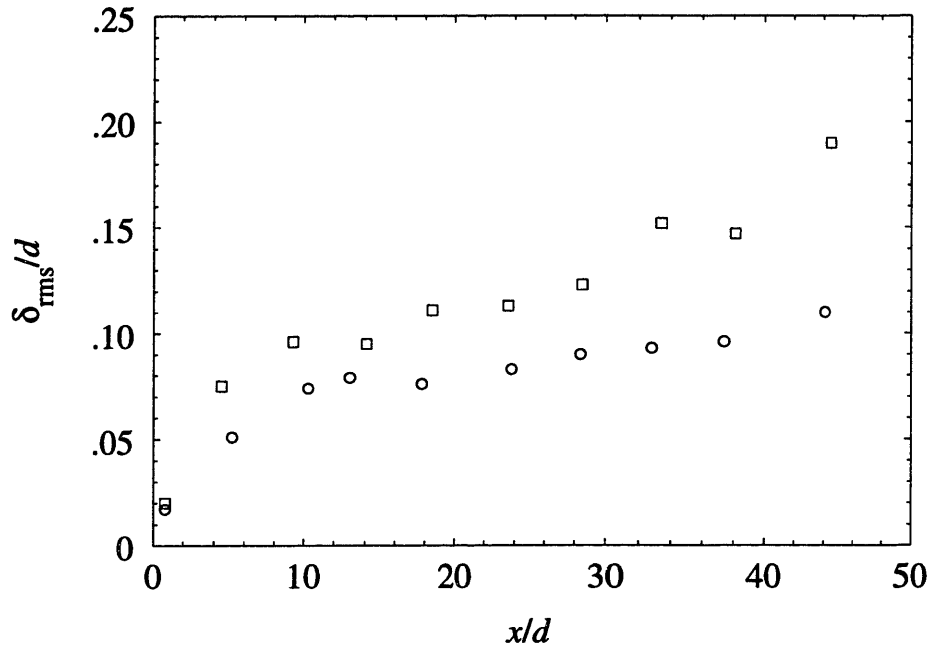
Figure 3-13: The amplitude of free surface disturbances on the the jets of 10% isopropanol-water solution ($\sigma = 0.042$ N/m).
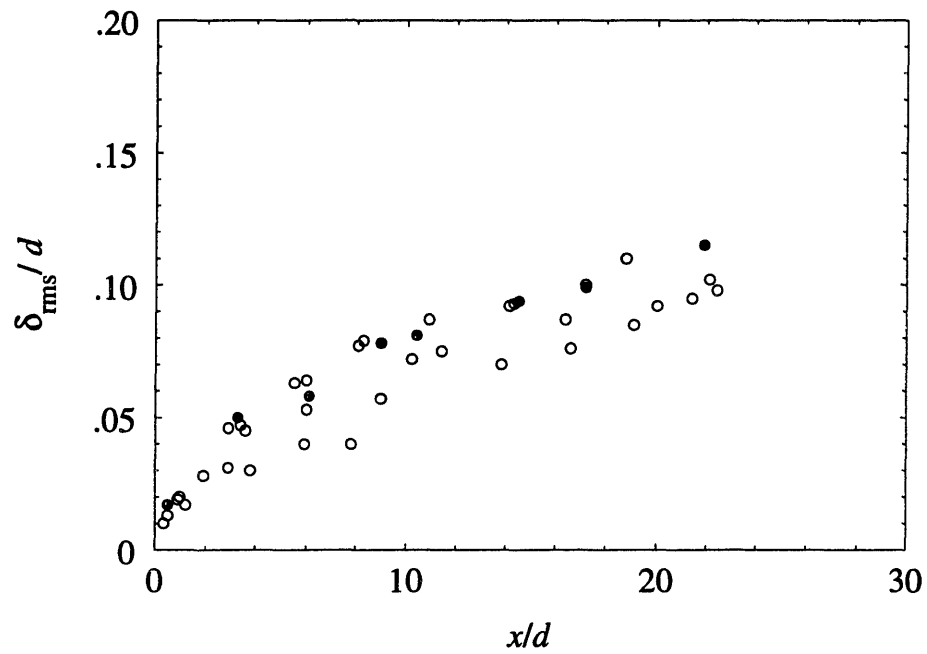
Figure 3-14: Surfactants do not alter the turbulent jet surface disturbances. The Weber number of the soap-water jet is based on the surface tension of the surfactant-saturated surface. The Weber number in parenthesis is based on the surface tension of pure water.
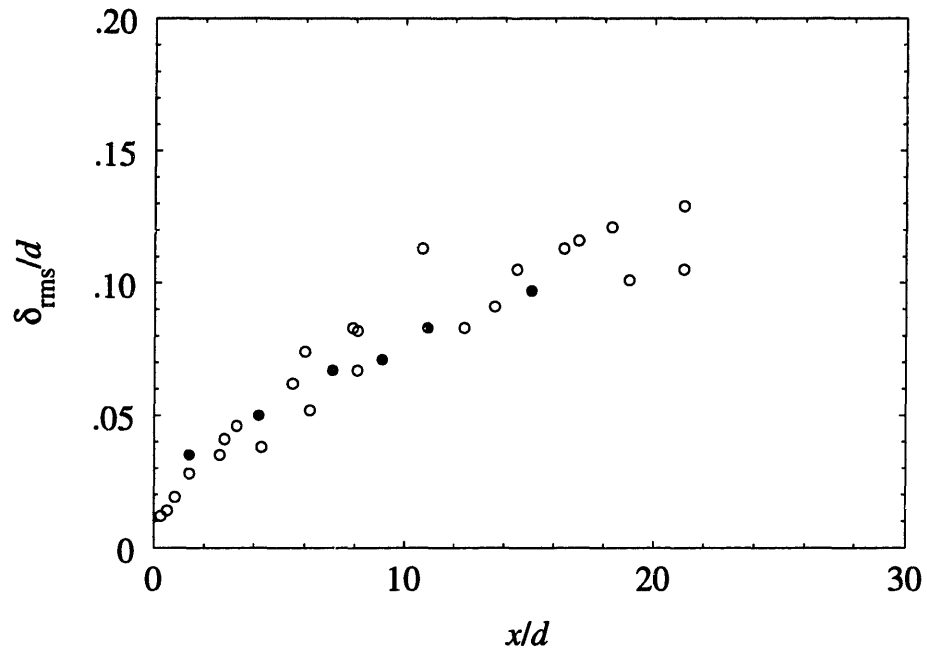
Figure 3-15: Surfactants do not alter the turbulent jet surface disturbances. The Weber number of the soap-water jet is based on the surface tension of the surfactant-saturated surface. The Weber number in parenthesis is based on the surface tension of pure water.
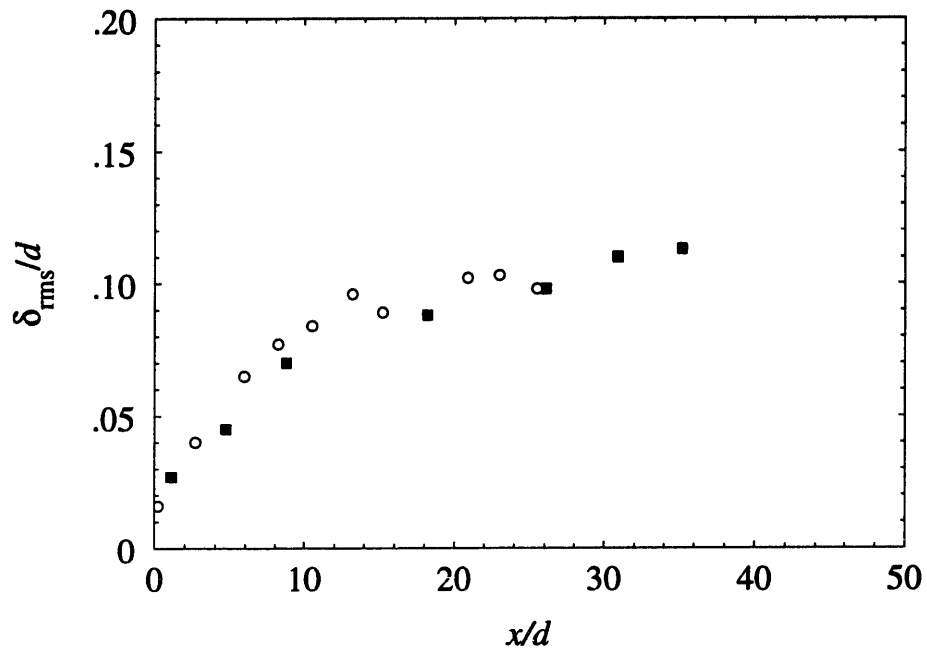
Figure 3-16: Surfactants do not alter the turbulent jet surface disturbances. The Weber number of the soap-water jet is based on the surface tension of the surfactant-saturated surface. The Weber number in parenthesis is based on the surface tension of pure water.
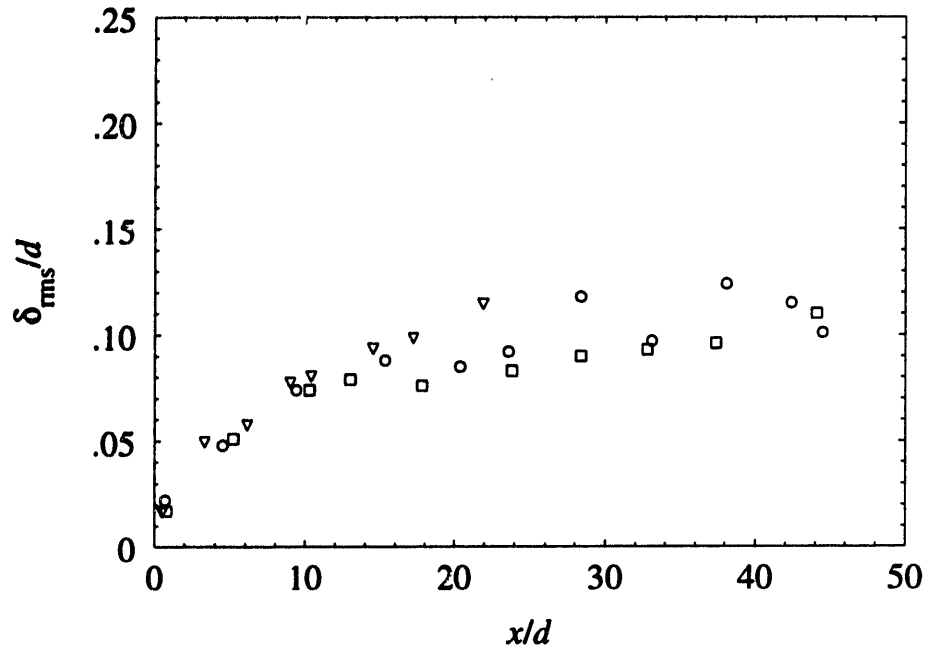
Figure 3-17: The jet Weber number correlates the variation of the amplitude of disturbances for different fluid systems.
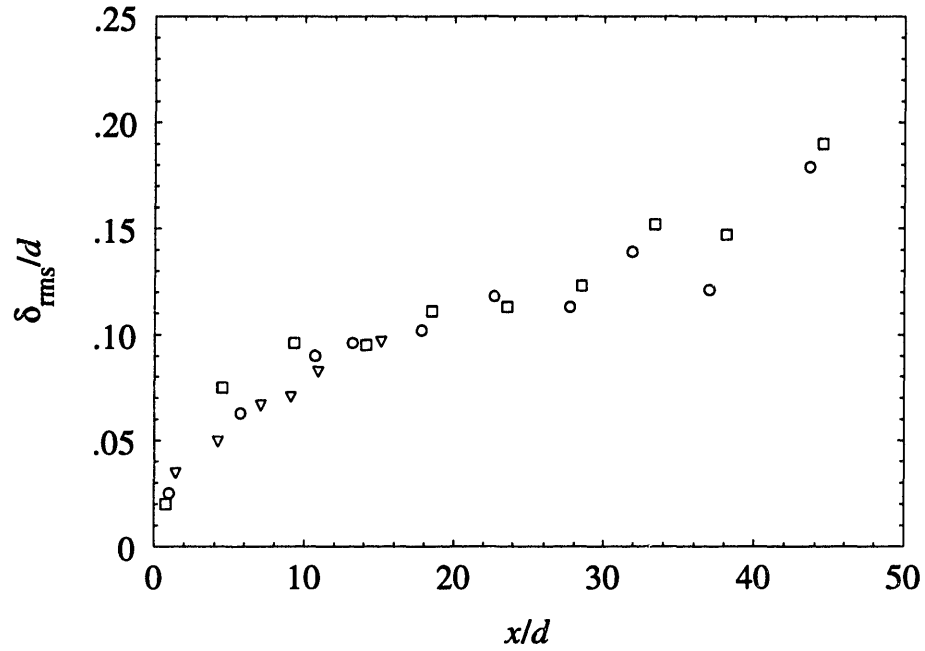
Figure 3-18: The jet Weber number correlates the variation of the amplitude of disturbances for different fluid systems.

3.3.3 The effect of additives

Some of the additives that reduce drag in turbulent pipe flow are also known to change considerably the structure of disturbances on the high velocity free-surface turbulent liquid jets (Hoyt et al. 1974) and reduce their tendency to break up (Bhunia and Sonin, 1993). Tests were done with a drag reducing additive, guar, which is a plant polysaccharide (obtained from *Cyamopsis tetragonolobus*). A concentration of 500 weight-parts-per-million (wppm) of guar in water was used for the solution, which is in the range where it is most effective as a drag reducer (Hoyt 1985). The surface tension of this guar solution was measured to be 0.052 N/m. A comparison of the rms amplitude of disturbances on guar-water jets with pure water jets are shown in Figure 3-19. Lack of any significant change in the amplitude of surface disturbances may indicate a higher concentration threshold of guar additive for any change in jet characteristics than in case of pipe flows.

3.4 A model for turbulent free surface disturbances

Let us consider a turbulent free surface of infinite dimensions with turbulent liquid of infinite depth on one side of it. A rectangular Cartesian coordinate system is positioned so that the $x - y$ plane coincides with the mean location of the free surface and the z axis points away from the liquid side ($-z$ represents the depth of the liquid below the free surface). Let $\delta(x, y, t)$ be the instantaneous amplitude of surface disturbances above the mean free surface and $p(x, y, z, t)$ be the fluctuating component of pressure at any location (x, y, z). Since the pressure fluctuations on the free surface are balanced by the surface tension, we have at $z \cong 0$

$$p = -\sigma \left(\frac{\partial^2 \delta}{\partial x^2} + \frac{\partial^2 \delta}{\partial y^2} \right) \tag{3.2}$$
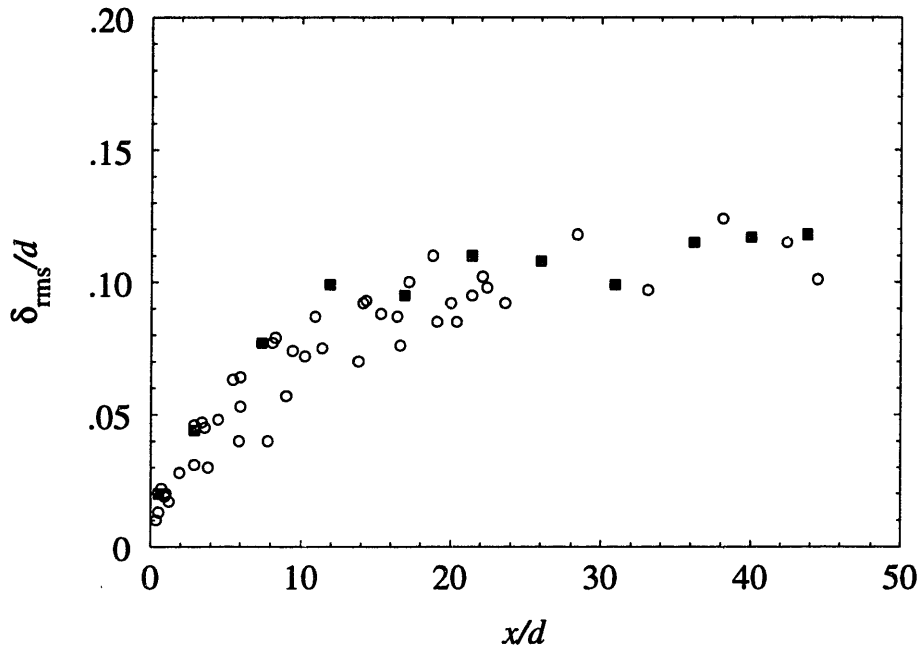
Figure 3-19: The presence of 500 wppm guar in water does not alter the amplitude of jet surface disturbances

Let us define Fourier transforms of δ and p as follow:

$$\delta = \int_{-\infty}^{\infty} \int_{-\infty}^{\infty} \Delta(k_1, k_2, t) e^{-i(k_1 x + k_2 y)} dk_1 dk_2 \tag{3.3}$$

and

$$p = \int_{-\infty}^{\infty} \int_{-\infty}^{\infty} \int_{-\infty}^{\infty} P(k_1, k_2, k_3, t)$$
$$\times e^{-i(k_1 x + k_2 y + k_3 z)} dk_1 dk_2 dk_3 \tag{3.4}$$

Substituting in Equation 3.2 we get,

$$\int_{-\infty}^{\infty} P(k_1, k_2, k_3, t) dk_3 = \sigma(k_1^2 + k_2^2) \Delta(k_1, k_2, t) \tag{3.5}$$

To describe any time-evolution of the statistical moments of δ and p, the Navier-Stokes equation with proper boundary and initial conditions must be used. In this model we restrict our attention to the instantaneous relation between p and δ. Specifically, we suppose the statistics to be taken over spatial intervals large compared to the turbulent integral scales but small compared to the axial distance over which the surface disturbances evolve significantly. In practice, this means wavelengths of a few jet diameters or less. Since the actual measurements are time averages taken at a single spatial location, we are applying the usual Taylor hypothesis (Monin and Yaglom, 1975, Vol. 2, pg. 449) to obtain the wavenumber spectrum from the frequency spectrum with frequency $= u k_1$. This makes the statistics of p and δ in the subsequent analysis instantaneous spatial averages with each measured parameter corresponding to its time average at any spatial location.

Assuming the turbulent pressure fluctuations to be a spatially-homogeneous random process the turbulent pressure spectrum, $F(k)$, is defined by

$$\overline{p^* p} = \int_{-\infty}^{\infty} \int_{-\infty}^{\infty} \int_{-\infty}^{\infty} F(k) dk_1 dk_2 dk_3 \tag{3.6}$$

where the * indicates a complex conjugate. Assuming both δ and p to be stationary

random functions, and multiplying Equation 3.5 with its complex conjugate, we get

$$\overline{\delta^2} = \int_{-\infty}^{\infty} \int_{-\infty}^{\infty} \frac{1}{\sigma^2 (k_1^2 + k_2^2)^2} \int_{-\infty}^{\infty} F(k) dk_3 dk_2 dk_1 \qquad (3.7)$$

For isotropic, homogeneous turbulence (George et al., 1984),

$$F(k) \sim 0.26 \rho^2 u'^4 l^3 (kl)^{-13/3}, \quad kl \gg 1$$

where u' is the fluctuating component of turbulent velocity and l is the integral scale of turbulence.

Let us define the spectrum of disturbances, $G(\eta)$ by the following equation:

$$\frac{\overline{\delta^2}}{l^2} = \int_0^{\infty} G(\eta) d\eta \qquad (3.8)$$

where, η is the wavenumber of the free surface disturbances non-dimensionalized by the integral scale of turbulence, l. From Equations 3.7 and 3.8 it follows that at high wavenumbers the disturbance spectrum is

$$G(\eta) \sim 0.26 \times 2\pi \frac{\rho^2 u'^4}{\sigma^2} \frac{l^{-13/3}}{k_p^3} \int_{-\infty}^{\infty} \frac{dk_3}{(k_p^2 + k_3^2)^{13/6}}, \qquad \eta \gg 1 \qquad (3.9)$$

where we have used the $(k_1, k_2) \leftrightarrow (k_p, \theta)$ Cartesian to polar coordinate transformation in the wavenumber plane with $\eta = k_p l$. Upon evaluating the integral, the spectrum of free surface turbulent disturbances is given by

$$G(\eta) \sim 2.41 \frac{\rho^2 u'^4 l^2}{\sigma^2} \eta^{-19/3}, \qquad \eta \gg 1 \qquad (3.10)$$

This explains the observed -19/3 slope in the log-log plot of the disturbance spectra. It should be noted that this is the *steepest possible slope* before the Kolmogorov scale. For free surfaces with a significant amount of shear, we should expect different slopes at high wavenumber in the spectra of disturbances since the corresponding pressure spectra have different slopes (George et al., 1984). Therefore, in the case of jets, near the nozzle we should see slopes different from -19/3 at high wavenumbers.

These conclusions are confirmed by the measured spectra (Figures 3-10, 3-11 and 3-12).

3.5 Conclusions

A non-intrusive, optical technique to measure the instantaneous amplitude of surface disturbances on turbulent liquid jets has been applied to obtain the evolution of surface roughness. The surface disturbance spectrum has also been measured and a simple theory developed for its high wavenumber decay.

- Measurements show a non-exponential (i.e. non-Rayleigh type) growth of the rms amplitude of jet surface disturbances as it moves downstream.

- A good correlation between the amplitude of turbulent jet surface disturbances and the fraction of liquid splattered in jet impingement is observed.

- The spectra of jet surface disturbances show that in turbulent jets, turbulent disturbances dominate over any single-wavelength Rayleigh-type unstable disturbances. The slope of the log-log plot of the spectra of disturbances at high wavenumber is -19/3. Near the nozzle slopes are different at high wavenumbers because of significant amount of energy dissipation by shear forces.

- Presence of a surfactant in the jet liquid does not alter the rms amplitude of turbulent disturbances. The characteristic Weber number, for scaling the axial variation of the rms amplitude of turbulent jet surface disturbances, even for surfactant-laden jets should be based on the surface tension of the bulk liquid alone.

- A mathematical model of free surface turbulence presented here, correctly predicts the observed $k_p^{-19/3}$ high wavenumber variation of the disturbance spectra.

Chapter 4

References

Batchelor, G. K., 1953, *The Theory of Homogeneous Turbulence*, Cambridge University Press.

Bhunia, S. and Sonin, A.A., 1993, "Material removal by high speed water jets: some basic experiments," *J. Fluids Engg.*, Trans. ASME (final manuscript in preparation)

Chen, T.-F. and Davis, J.R., 1964, "Disintegration of a turbulent water jet", *Journal of Hydraulics Division, Proceedings of ASCE*, HY 1, January 1964, pp.175 – 206.

Drazin, P.G. and Reid, W.H., 1981, *Hydrodynamic Stability*, Cambridge University Press.

Errico, M., 1986, *A study of the interaction of liquid jets with solid surfaces*, Ph.D. thesis, University of California, San Diego.

George, W.K., Beuther, P.D. and Arndt, R.E.A., 1984, "Pressure spectra in turbulent free shear flows", *J. Fluid Mech.*, Vol. 148.

Hoyt, J.W., 1985, "Drag reduction in polysaccharide solutions", Trends in Biotechnology, Vol. 3, No., 1.

Hoyt, J.W., Taylor, J.J. and Runge, C.D., 1974, "The structure of jets of water and polymer solution in air", *J. Fluid Mech.*, Vol. 63, pp. 635 – 640.

Kim, S. and Mills, A.F., 1989a, "Condensation on coherent turbulent liquid jets: part I – experimental study", *J. Heat Transfer*, Trans. ASME, Vol. 111, November 1989, pp. 1068 – 1074.

Kim, S. and Mills, A.F., 1989b, "Condensation on coherent turbulent liquid jets: part II – a theoretical study", *J. Heat Transfer*, Trans. ASME, Vol. 111, November 1989, pp.1075 – 1082.

Köhler, J., 1993, *Heat and mass transfer in a two-phase flow of a binary mixture*, Heat Transfer Lab. Internal Report, Department of Mechanical Engineering, MIT, Cambridge, MA.

Laufer, J., 1954, "The structure of turbulence in fully developed pipe flow", NACA Technical Report No. 1174.

Lienhard, J.H. and Day, J.B., 1970, "The breakup of superheated liquid jets", *Journal of Basic Engineering*, Transactions of ASME, pp. 515–522.

Lienhard V, J.H., Liu, X. and Gabour, L.A., 1992, "Splattering and heat transfer during impingement of a turbulent liquid jet", *Journal of Heat Transfer*, Transactions of ASME, Vol. 114, May 1992, pp. 362–372.

Miesse, C.C., 1955, "Correlation of experimental data on the disintegration of liquid jets", *Industrial and Engineering Chemistry*, Vol. 47, September 1955, pp.1690–1701.

Monin, A.S. and Yaglom, A.M., 1975, *Statistical Fluid Mechanics: Mechanics of Turbulence*, Vol. 2, pg. 449, The MIT Press.

Stevens, J. and Webb, B.W., 1989a, "Local heat transfer coefficients under an axisymmetric, single-phase liquid jet", *Heat Transfer in Electronics – 1989*, ASME HTD, Vol. 111, pp.113–119 (National Heat Transfer Conference, Philadelphia, PA).

Stevens, J. and Webb, B.W., 1989b, "Measurements of the free surface flow structure under an impinging, free liquid jet", *Proc. 3rd ASME/JSME Thermal Eng. Joint Conf.*, Reno, NV.

Tadrist, L., Alaoui, E.K.O., Occelli, R. and Pantaloni, J., 1991, "Experimental study of a liquid jet flowing into another immiscible liquid 'A local analysis of the interface'," *Experiments in Fluids*, Vol. 12, pp.67 – 75.

Varela, D. A. and Lienhard V, J. H., "Development of non-linear waves on a non-uniform axisymmetric film", *Bulletin of American Physical Society*, AI8, Vol 36, No. 10; 44th Annual Meeting of Division on Fluid Dynamics, Scottsdale, November 1991.

Weber, C., 1931, "Zum Zerfall eines Flüssigkeitsstrahles", *Zeitschrift für angewandte Mathematik und Mechanik*, Vol. 2, pp.136–154.

Wolf, D. H., Viskanta, R. and Incropera, F. P., 1990, "Local convective heat transfer from a heated surface to a planar jet of water with a nonuniform velocity profile", *J. Heat Transfer*, Trans. ASME, Vol. 112, November 1990, pp. 899–905.

Womac, D. J., Aharoni, G., Ramadhyani, S. and Incropera, F. P., 1990, "Single phase liquid jet impingement cooling of small heat sources", *Proc. 9th International Heat Transfer Conference*, Jerusalem, Israel, Vol. 4, pp.149–154.

Appendix A

Estimation of Diffusion of Surfactants to a Turbulent Free Surface Excluding Reentrainment Effects

The flux of surfactant reaching the free surface is given by:

$$j = h_D m_\infty \tag{A.1}$$

where, h_D is the coefficient of mass transfer to the free surface. Note that m_∞, the mass fraction of the surfactant species away from the free surface, taken to be same as the bulk mass fraction of the surfactant, is used as the mass transfer driving force. Under this model, we assume that the free surface captures all the solute molecules that reach it, resulting in a near zero concentartion of solute in the liquid at the interface. This should provide a conservative or under estimate of the time (or the distance from the nozzle exit) that it will take for the free surface to reach a desired surface concentration. To calculate the coefficient of mass transfer to a turbulent free

surface we use the correlation developed by Köhler (1993):

$$\text{Sh}_t = \frac{4}{3\sqrt{\pi}} \left(1 + 0.4 \frac{\text{Re}_t}{\text{Re}_t^*}\right) \text{Re}_t^{0.5} \text{Sc}^{0.5} \qquad \text{(A.2)}$$

where, $\text{Sh}_t = h_D l / \rho \mathcal{D}$ is the turbulent Sherwood number, $\text{Re}_t = u'l/\nu$ is the turbulent Reynolds number, $\text{Re}_t^* = 800$, $\text{Sc}=\nu/\mathcal{D}$ is the Schmidt number, l is the integral scale of turbulence, $\mathcal{D}$ is the diffusion coefficient of the surfactant-liquid mixture and ν is the liquid kinematic viscosity.

The surface concentration of the adsorbed monolayer of surfactants at a distance, x from the nozzle,

$$J = j \frac{x}{u_f} = \text{Sh}_t \frac{\mathcal{D}}{l} c_\infty \frac{x}{u_f} \qquad \text{(A.3)}$$

Therefore the distance from the nozzle exit at which a certain level of surface concentration, J is reached is given by:

$$\frac{x}{d} = \frac{Jl\,u_f}{\text{Sh}_t c_\infty\, d\,\mathcal{D}} \qquad \text{(A.4)}$$

Sodium dodecyl sulfate [$\text{CH}_3(\text{CH}_2)_{11}\text{SO}_4\text{Na}$] is representative of the type of surfactants used here. It requires a surface concentration of the order of 1 mg/m^2 to lower the surface tension by about 50%. We estimate, $l \sim 0.5d$, $u' \approx 0.04u_f$, $\mathcal{D} \sim 10^{-9}\text{m}^2/\text{s}$, $\nu \approx 10^{-6}\text{m}^2/\text{s}$ and $m_\infty \approx 2 \times 10^{-3}$. Therefore for the two cases of surfactant-laden jets in Figure 2-11, to reach $J \sim 10^{-6}$ kg/m^2, x/d has to be of the order of 3-4.

Appendix B

Mathematical Model of Surface Disturbance Evolution on a Turbulent Liquid Jet in Gas

Turbulent disturbances dominate the surface structure of a turbulent liquid jet in air, especially near the nozzle. Turbulence provides an initial spectrum of disturbances present in the jet. The growth rates of surface disturbances on these jets are given approximately by Rayleigh's analysis. Following the same approach we can analyse the jet from a reference frame moving with the mean axial velocity of the jet. In this frame the incompressible Navier-Stokes equation for the jet becomes,

$$\nabla^2 \tilde{p} = -\rho \frac{\partial^2}{\partial x_i \partial x_j}(u_i' u_j') = -\rho f(x, y, z, t) \tag{B.1}$$

where $\tilde{p} = p - \sigma/a$; p, σ and a are the instantaneous static pressure, surface tension and the undisturbed jet radius, respectively, and $\vec{u'}$ is the fluctuating component of the velocity.

The turbulent pressure field and hence the term on the right hand side of Equation B.1 can be considered "frozen" in time if the frequency of pressure fluctuations is much smaller than that of the oscillatory/unstable velocity modes. This is expected to hold only over a part of the spectrum of turbulent disturbances as will be shown

78

later.

For small amplitude of disturbances the linearized boundary conditions at $r = a$ are,

Kinematic:

$$u'_r = \frac{\partial \delta}{\partial t} \tag{B.2}$$

Pressure continuity:

$$\tilde{p} = -\sigma \left(\frac{\delta}{a^2} + \frac{\partial^2 \delta}{\partial x^2} + \frac{1}{a^2} \frac{\partial^2 \delta}{\partial \theta^2} \right) \tag{B.3}$$

Dynamic:

$$\frac{\partial u'_r}{\partial t} = -\frac{1}{\rho} \frac{\partial \tilde{p}}{\partial r} - \frac{\partial}{\partial x_j} (u'_r u'_j) \tag{B.4}$$

where δ is the instantaneous height of surface disturbance above the undisturbed radius and r measures the radial distance from the jet axis which is chosen to be along the x direction. The dynamic boundary condition assumes an inviscid flow.

Equation B.1 has been solved, neglecting the second term on the right hand side of Equation B.4. Using that result an evolution equation for the rms value of the surface disturbances can be found based on isotropic turbulence. Assuming 4% turbulence intensity, the solution is valid for

$$We_d \ll 2 \times 10^4 \eta_1 (\eta_1^2 + m^2 - 1) \tag{B.5}$$

where $\eta_1 = k_1 a$; k_1 being the wavenumber of disturbances in the axial plane of the jet, m($= 0,1,2.......$) stands for the disturbance modes in the radial plane of the jet. For most of the turbulent disturbance spectrum $\eta_1 \geq 1$. This estimate is derived by comparing the time scales of the most energetic turbulent eddies and of the growth rates for the corresponding wavelength of disturbances.

79

Details of the analysis

Equation B.1 can be written as,

$$\frac{1}{r}\frac{\partial}{\partial r}\left(r\frac{\partial \tilde{p}}{\partial r}\right) + \frac{1}{r^2}\frac{\partial^2 \tilde{p}}{\partial \theta^2} + \frac{\partial^2 \tilde{p}}{\partial x^2} = -\rho f(x,y,z) \tag{B.6}$$

As explained before, the time dependence of the function f can be neglected only for those disturbance wavelengths at which the disturbance growth rates are faster than the pressure fluctuations. The range of validity of this assumption is given by Ineqality B.5. Here both (r,θ) and (y,z) coordinates are used on the plane perpendicular to the jet axis such that $y = r\cos\theta$ and $z = r\sin\theta$.

Expanding both $\tilde{p}$ and f in Fourier integral-series,

$$\tilde{p}(x,y,z,t) = \int_{-\infty}^{\infty}\sum_{m=-\infty}^{\infty} A(k_1,r,m,t)e^{-im\theta}e^{-ik_1 x}dk_1 \tag{B.7}$$

$$f(x,y,z) = \int_{-\infty}^{\infty}\sum_{m=-\infty}^{\infty} B(k_1,r,m)e^{-im\theta}e^{-ik_1 x}dk_1 \tag{B.8}$$

and substituting in Equation B.6 we get,

$$\frac{1}{r}\frac{\partial}{\partial r}\left(r\frac{\partial A}{\partial r}\right) - \left(\frac{m^2}{r^2} + k_1^2\right)A(k_1,r,m,t) = -\rho B(k_1,r,m) \tag{B.9}$$

Since $A(k_1,0,m,t)$ is non-singular,

$$A(k_1,r,m,t) = \tilde{a}(k_1,m,t)I_m(k_1 r)$$
$$+ \int_0^r \rho B(k_1,\zeta,m)\zeta[I_m(k_1\zeta)K_m(k_1 r) - K_m(k_1\zeta)I_m(k_1 r)]d\zeta \tag{B.10}$$

where I_m and K_m are modified Bessel functions. The particular solution is obtained by the method of variation of parameters using the result that the Wronskian of $I_m(r)$ and $K_m(r)$ is $-1/r$.

Now we expand δ in Fourier integral-series

$$\delta(x,\theta,t) = \int_{-\infty}^{\infty}\sum_{m=-\infty}^{\infty} C(k_1,m,t)e^{-im\theta}e^{-ik_1 x}dk_1 \tag{B.11}$$

80

Substituting it in Equation B.3 and using Equations B.7 and B.9 we get,

$$-\sigma\left(\frac{1}{a^2} - k_1^2 - \frac{m^2}{a^2}\right)C(k_1,m,t) = A(k_1,a,m,t) = \tilde{a}(k_1,m,t)I_m(k_1a)$$
$$+ \int_0^a \rho B(k_1,\zeta,m)\zeta[I_m(k_1\zeta)K_m(k_1r) - K_m(k_1\zeta)I_m(k_1r)]d\zeta \quad \text{(B.12)}$$

As an approximation, let us simplify the dynamic boundary condition (Equation B.4) by neglecting the contribution of the Reynolds stress gradient at the jet surface to the acceleration of the fluid on the surface. This assumes the acceleration of the fluid on the jet surface to be due to pressure fluctuations, both turbulent and oscillatory, only. Combining it with the kinematic boundary condition (Equation B.2) we get at $r = a$

$$\frac{\partial^2\delta}{\partial t^2} = -\frac{1}{\rho}\frac{\partial\tilde{p}}{\partial r} \quad \text{(B.13)}$$

Eliminating $\tilde{a}$ between Equations B.10 and B.12, $A(k_1,r,m,t)$ can be expressed in terms of $C(k_1,m,t)$ and some known functions. Taking the Fourier transform of Equation B.13, as defined by Equations B.7 and B.11, and using the expression for $A(k_1,r,m,t)$ mentioned above we obtain the equation governing the growth of each Fourier component of surface disturbances,

$$\ddot{C} + q_1 C = q_2 \quad \text{(B.14)}$$

where,

$$q_1 = \frac{\sigma}{\rho a^3}\frac{\eta_1 I_m'(\eta_1)}{I_m(\eta_1)}(\eta_1^2 + m^2 - 1) \quad \text{(B.15)}$$

and

$$q_2 = \frac{1}{aI_m(\eta_1)}\int_0^a \zeta B(k_1,\zeta,m)I_m(k_1\zeta)d\zeta \quad \text{(B.16)}$$

Therefore,

$$C(k_1,m,t) = a_1\cos(\sqrt{q_1}t) + b_1\sin(\sqrt{q_1}t) + \frac{q_2}{q_1} \quad \text{(B.17)}$$

Using the initial conditions, $\delta(x,\theta,0) = \dot{\delta}(x,\theta,0) = 0$ we obtain $C(k_1,m,0) = \dot{C}(k_1,m,0) = 0$ from Equation B.11. Using those values in the above equation we obtain an expression for $C(k_1,m,t)$. Substituting that expression back into Equa-

81

tion B.11 we get,

$$\delta(x,\theta,t) = \int_{-\infty}^{\infty} \sum_{m=-\infty}^{\infty} \frac{2\sin^2(\sqrt{q_1}t/2)}{q_1}q_2 e^{-im\theta}e^{-ik_1x}dk_1 \qquad (\text{B.18})$$

Taking the ensemble average of the product of δ and its complex conjugate,

$$\overline{\delta^*\delta} = \overline{\delta^2} = \int_{-\infty}^{\infty} \sum_{m=-\infty}^{\infty} \frac{4\sin^4(\frac{1}{2}\sqrt{q_1}x/u_f)}{q_1^2}$$

$$\times \frac{1}{a^2 I_m^2(\eta_1)} \int_0^a \int_0^a \zeta\zeta_1 \overline{B^*(k_1,\zeta,m)B(k_1,\zeta_1,m)}I_m(k_1\zeta)I_m(k_1\zeta_1)d\zeta d\zeta_1 dk_1 \text{(B.19)}$$

Time t, as measured in the moving frame, is replaced by x/u_f in the above equation since the frame moves with velocity, u_f.

Evaluation of $\overline{B^*(k_1,\zeta,m)B(k_1,\zeta_1,m)}$

Let us consider two points in the turbulent flow, $\vec{X} \equiv \{x,y,z\} \equiv \{x,\zeta,\theta\}$ and $\vec{X_1} \equiv \{x_1,y_1,z_1\} \equiv \{x_1,\zeta_1,\theta_1\}$ such that $\vec{X_1} - \vec{X} \equiv \{x',y',z'\} \equiv \{x',\zeta',\theta'\}$. Here $\{x,y,z\}$ and $\{x,\zeta,\theta\}$ describe the coordinates in cartesian and cylindrical systems respectively. Therefore $y = \zeta\cos\theta$, $z = \zeta\sin\theta$ and so on. Now assuming the turbulence to be homogeneous $f(x,y,z)$ becomes a stationary random function. Therefore,

$$\int_{-\infty}^{\infty} \sum_{m=-\infty}^{\infty} \overline{B^*(k_1,\zeta,m)B(k_1,\zeta_1,m)}e^{-im\theta'}e^{-ik_1x'}dk_1$$

$$= \overline{f^*(\vec{X})f(\vec{X_1})}$$

$$= \int_{-\infty}^{\infty} \int_0^{\infty} \int_0^{2\pi} F(k)e^{-ik_1x'-i\{k_2(y_1-y)+k_3(z_1-z)\}}d\theta_k k_\perp dk_\perp dk_1$$

$$= \int_{-\infty}^{\infty} \int_0^{\infty} \int_0^{2\pi} F(k)e^{-ik_1x'}e^{-ik_\perp\{\cos\theta_k(\zeta_1\cos\theta_1-\zeta\cos\theta)+\sin\theta_k(\zeta_1\sin\theta_1-\zeta\sin\theta)\}}d\theta_k k_\perp dk_\perp dk_1$$

Assuming an isotropic turbulent velocity field, $F(k)$ is the isotropic spectrum function of the correlation function $\overline{f^*(\vec{X})f(\vec{X_1})}$. The wavenumber $k = |\vec{k}|$. The wavevector $\vec{k}$ can be resolved into components k_1,k_2,k_3 corresponding to x,y,z directions respectively or into components $k_1,k_\perp,\theta_k$ corresponding to x,r,θ directions respectively.

82

Therefore from the above equation,

$$\sum_{m=-\infty}^{\infty} \overline{B^*(k_1,\zeta,m)B(k_1,\zeta_1,m)}e^{-im\theta'} = \int_0^{\infty}\int_0^{2\pi} F(k)e^{-ik_\perp\{\zeta_1\cos(\theta_k-\theta_1)-\zeta\cos(\theta_k-\theta)\}}d\theta_k k_\perp dk_\perp$$

(B.20)

The left hand side of the above equation being a Fourier series,

$$\overline{B^*(k_1,\zeta,m)B(k_1,\zeta_1,m)}$$

$$= \frac{1}{2\pi}\int_0^{\infty}\int_0^{2\pi}\int_0^{2\pi} F(k)e^{-ik_\perp\{\zeta_1\cos(\theta_k-\theta-\theta')-\zeta\cos(\theta_k-\theta)\}+im\theta'}d\theta'd\theta_k k_\perp dk_\perp$$

$$= \frac{1}{2\pi}\int_0^{\infty}\int_0^{2\pi} F(k)e^{ik_\perp\zeta\cos(\theta_k-\theta)-im(\theta_k-\theta)}\int_0^{2\pi}e^{-ik_\perp\zeta_1\cos(\theta'+\theta-\theta_k)+im(\theta'+\theta-\theta_k)}d\theta'd\theta_k k_\perp dk_\perp$$

$$= i^m\int_0^{\infty}\int_0^{2\pi} F(k)e^{ik_\perp\zeta\cos(\theta_k-\theta)-im(\theta_k-\theta)}J_m(-k_\perp\zeta_1)d\theta_k k_\perp dk_\perp$$

$$= 2\pi\int_0^{\infty} F(k)J_m(k_\perp\zeta)J_m(k_\perp\zeta_1)k_\perp dk_\perp$$

(B.21)

since $\int_0^{2\pi} e^{im\theta+is\cos\theta}d\theta = 2\pi i^m J_m(s)$, where J_m is a Bessel function of first kind.
Therefore,

$$\int_0^a\int_0^a \zeta\zeta_1\overline{B^*(k_1,\zeta,m)B(k_1,\zeta_1,m)}I_m(k_1\zeta)I_m(k_1\zeta_1)d\zeta d\zeta_1$$

$$= \int_0^{\infty} 2\pi F(k)k_\perp\left[\int_0^a \zeta J_m(k_\perp\zeta)I_m(k_1\zeta)d\zeta\right]^2 dk_\perp$$

(B.22)

Evaluation of $F(k)$

Following the analysis of Batchelor (1953) and George et al. (1984) we can obtain
an expression for $F(k)$. Let us define the Fourier transform of the two point, fourth
moment of velocity as follows:

$$\overline{u_i(\vec{X})u_j(\vec{X})u_k(\vec{X'})u_l(\vec{X'})} - \overline{u_i(\vec{X})u_j(\vec{X})}.\overline{u_k(\vec{X'})u_l(\vec{X'})} = \int F_{ij,kl}(\vec{k})e^{-i\vec{k}.(\vec{X'}-\vec{X})}d\vec{k}$$

(B.23)

where the integral is taken over the entire wavenumber space. The second term on
the left hand side of the above equation being constant in a homogeneous turbulent

83

field

$$\overline{\frac{\partial^2}{\partial x_i \partial x_j}\{u_i'(\vec{X})u_j'(\vec{X})\}\frac{\partial^2}{\partial x_k' \partial x_l'}\{u_k'(\vec{X'})u_l'(\vec{X'})\}} = \int k_i k_j k_k k_l F_{ij,kl}(\vec{k})e^{-i\vec{k}\cdot(\vec{X'}-\vec{X})}d\vec{k}$$

(B.24)

As shown by Batchelor (1953, pp. 180),

$$k_i k_j k_k k_l F_{ij,kl}(\vec{k}) = \frac{k^4}{8\pi^2}\int E(k')E(|\vec{k}-\vec{k}'|)\frac{\sin^4\phi}{|\vec{k}-\vec{k}'|^4}d\vec{k}'$$

(B.25)

Comparison of this equation with Equation B.24 provides us with an expression for the rms amplitude of the turbulent liquid jet surface disturbances

$$\frac{\sqrt{\bar{\delta^2}}}{d} = \mathrm{We}_d\left(\frac{u'}{u_f}\right)^2\sqrt{\pi\int_0^\infty \sum_{m=-\infty}^\infty \frac{\sin^4\left(\sqrt{\frac{2s}{\mathrm{We}_d}}\frac{x}{d}\right)}{s^2 I_m^2(\eta_1)}L(\eta_1)d\eta_1}$$

(B.26)

where, $\eta = ka$, $\eta_1 = k_1 a$ and $\eta_\perp = k_\perp a$ i.e. $\eta = \sqrt{\eta_1^2 + \eta_\perp^2}$,

$$s = \eta_1(\eta_1^2 + m^2 - 1)\frac{I_m'(\eta_1)}{I_m(\eta_1)}$$

(B.27)

and

$$L(\eta_1) = \frac{a}{u'^4}\int_0^\infty \mathcal{F}(\eta)\eta_\perp\left[\int_0^1 \phi J_m(\eta_\perp\phi)I_m(\eta_1\phi)d\phi\right]^2 d\eta_\perp$$

(B.28)

where, $F(k) = \mathcal{F}(\eta)$.

An expression for $F(k)$ given by George et al. (1984), is mentioned in Section 3.4.